

UC Santa Barbara

UC Santa Barbara Previously Published Works

Title

Activated Src kinase promotes cell cannibalism in Drosophila.

Permalink

<https://escholarship.org/uc/item/1zk318ws>

Journal

Journal of Cell Biology, 222(11)

Authors

Torres, Alba

Nano, Maddalena

Campanale, Joseph

et al.

Publication Date

2023-11-06





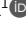
DOI

10.1083/jcb.202302076

Peer reviewed

ARTICLE

Activated Src kinase promotes cell cannibalism in *Drosophila*

Alba Yurani Torres¹, Maddalena Nano¹, Joseph P. Campanale¹, Sierra Deak¹, and Denise J. Montell¹

Src family kinases (SFKs) are evolutionarily conserved proteins acting downstream of receptors and regulating cellular processes including proliferation, adhesion, and migration. Elevated SFK expression and activity correlate with progression of a variety of cancers. Here, using the *Drosophila melanogaster* border cells as a model, we report that localized activation of a Src kinase promotes an unusual behavior: engulfment of one cell by another. By modulating Src expression and activity in the border cell cluster, we found that increased Src kinase activity, either by mutation or loss of a negative regulator, is sufficient to drive one cell to engulf another living cell. We elucidate a molecular mechanism that requires integrins, the kinases SHARK and FAK, and Rho family GTPases, but not the engulfment receptor Draper. We propose that cell cannibalism is a result of aberrant phagocytosis, where cells with dysregulated Src activity fail to differentiate between living and dead or self versus non-self, thus driving this malignant behavior.

Introduction

Src family kinases (SFKs) are a family of non-receptor, membrane-associated, tyrosine kinases. There are nine members in vertebrates where SRC, FYN, and YES are ubiquitously expressed, and FGR, HCK, LCK, BLK, LYN, and FRK are restricted to hematopoietic cells (Thomas and Brugge, 1997). All family members contain a conserved domain structure (Fig. 1 A) that includes four Src homology (SH) domains. Crystal structures of SFKs reveal closed and open conformations, corresponding to the inactive and active states, respectively (Sicheri and Kuriyan, 1997; Fig. 1 B).

SRC undergoes negative and positive regulation (Fig. 1 B). In the absence of stimulation, a large fraction of human SRC is inhibited by Tyr530 phosphorylation by the regulators C-terminal SRC Kinase (CSK) and CSK-homologous kinase (CHK; Zheng et al., 2000). SRC has been modeled as a “graded” kinase (Bradshaw, 2010) with sequential events enhancing its activity, culminating with trans-autophosphorylation of Tyr419 in the kinase domain (Harrison, 2003; Roskoski et al., 2015).

Active SFKs interact directly or indirectly with signaling receptors, signal transducers, adhesion molecules, cytoskeletal elements, and transcription factors, and they have been implicated in diverse biological functions, including proliferation and migration. While most studies in cell signaling focus on the role of SFKs in those processes, SFKs also function in recognition and phagocytosis of foreign pathogens and dead or damaged cells (Lowell, 2011; Wetzel et al., 2016), and have been implicated in

invasion and metastasis (Martellucci et al., 2020). In particular, SRC overexpression and elevated activity correlate with tumor progression and poor prognosis of numerous solid cancers as well as leukemias, lymphomas, and other hematological malignancies (Martellucci et al., 2020; Turro et al., 2016; Wheeler et al., 2009). Understanding the effects of SFKs in vivo is thus of great importance. However, it is challenging to dissect due to (1) the diverse consequences of SFK activation, (2) the number of SFK members, and (3) the number and variety of cells present in tumors and the challenges to high-resolution imaging in native tissues.

An emerging concept in cancer research is that polyclonal clusters of cells are major drivers of metastasis (Aceto et al., 2014; Cheung et al., 2016; Gundem et al., 2015; Kok et al., 2021; Maddipati and Stanger, 2015). In at least some types of cancer, clusters of cells are 60–100 times more effective at seeding metastases than single disseminated cells. Therefore, understanding the behavior of heterotypic cell clusters is of interest. However, the effects of activated SRC in heterotypic groups of cells in native 3D tissues have lagged behind studies of cultured cell lines.

Drosophila border cells migrate collectively as a group of four to six motile cells that surround and carry two immobile polar cells during oogenesis (Montell et al., 2012). This cell group serves as an excellent model for deciphering the molecular regulation of collective cell behaviors in 3D using a combination

¹Molecular, Cellular, and Developmental Biology Department, University of California, Santa Barbara, Santa Barbara, CA, USA.

Correspondence to Denise J. Montell: dmontell@ucsb.edu.

© 2023 Torres et al. This article is distributed under the terms of an Attribution–Noncommercial–Share Alike–No Mirror Sites license for the first six months after the publication date (see <http://www.rupress.org/terms/>). After six months it is available under a Creative Commons License (Attribution–Noncommercial–Share Alike 4.0 International license, as described at <https://creativecommons.org/licenses/by-nc-sa/4.0/>).

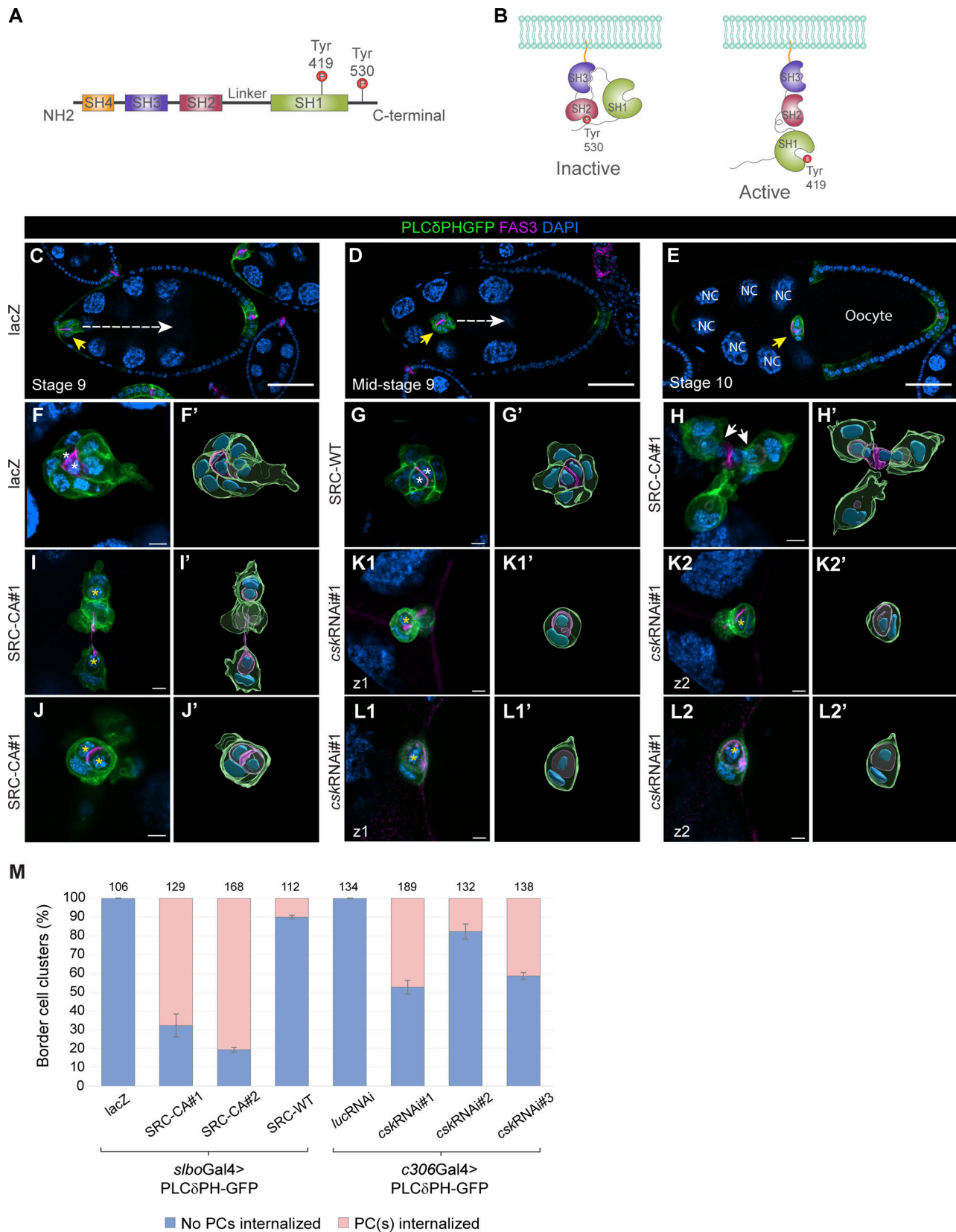


Figure 1. **Deregulated SRC activity causes border cells to engulf polar cells.** (A) Schematic representation of the domains found in human SRC kinase and the important regulatory sites of tyrosine phosphorylation in the SH1 domain (Tyr419) and in the C-terminal tail (Tyr530). (B) Schematic representation of intramolecular interactions of human SRC in inactive and active conformations. (C-E) Single sections from confocal images of egg chambers at stages 9 and 10 expressing UAS-PLCδPHGFP to label membranes and UAS-lacZ as a negative control. Egg chambers were stained with FAS3 (magenta) and DAPI (blue). Yellow

arrows point to the border cell cluster, and dashed white arrows indicate the migration path. NC: nurse cell nuclei. Scale bar, 50 μm . **(F–L2)** Single sections from confocal images of border cell clusters from egg chambers at stage 9 or 10 expressing UAS-PLC δ PHGFP and the indicated UAS transgenes. Polar cells are identified by FAS3 (magenta) and DAPI labels DNA (blue). White asterisks in F and G indicate non-internalized polar cells and yellow asterisks in I, J, K1, K2, L1, and L2 indicate internalized polar cells. **(H)** White arrows in H point to polar cell nuclei being pinched by border cells. **(K1 and K2)** Images show two different focal planes of the same cluster, as well as L1 and L2 images. Scale bar: 5 μm . **(F'–L2')** Segmentation and 3D reconstructions of the images in F–L2. **(M)** Quantifications of polar cell internalization from egg chambers at stage 10 of the indicated genotypes. Error bars: mean \pm SEM ($n = 3$ independent experiments). The total number of clusters analyzed (n) is indicated at the top of each bar.

of live imaging and genetics. Here, we use the border cells to study the consequences of elevated Src activity in one cell type on its interactions with another in vivo.

Outer, migratory border cells normally scoop up and carry the polar cells in between the adjacent germ cells, called nurse cells, until they reach the oocyte (Fig. 1, C–E). We found that elevated Src activity in outer border cells, either by down-regulation of *csk* or by expression of a constitutively activated form of Src42A, resulted in a surprising phenotype. Border cells with highly localized Src activity actively engulfed their living polar cell neighbors. The internalization of a passive cellular target by a non-professional phagocyte is called cell cannibalism, and it is always pathological (Borensztein et al., 2021). For instance, cell cannibalism can enhance the metastatic properties of breast cancer cells (Chen et al., 2019) and is used by melanoma cells for the double purpose of destroying lymphocytes and obtaining nutrients (Lugini et al., 2006). Importantly, cell cannibalism is often associated with metastatic behavior (Chen et al., 2019; Lugini et al., 2006). We show that, in border cells, Src-mediated cannibalism required integrin receptors, *Drosophila* SH2 ankyrin repeat kinase (SHARK) and focal adhesion kinase (FAK), and the Rac and Rho GTPases. Remarkably, border cells containing engulfed polar cells were still able to migrate. Together, these findings suggest a novel mechanism by which elevated Src kinase activity might promote cancer malignancy.

Results

Deregulated Src activity causes border cells to engulf polar cells

To assess the effects of increasing Src expression in border cells, we overexpressed a wild-type form of Src42A (hereafter, Src-WT). To increase Src activity, we used two different lines of a constitutively activated form of Src42A (hereafter, Src-CA#1 and Src-CA#2) as well as three different RNAi lines against C-terminal Src Kinase (*Csk*; *cskRNAi*#1–3), which is the sole known negative regulator of *Drosophila* Src activity (Pedraza et al., 2004; Stewart et al., 2003). We used *slbo*-Gal4, which drives the expression of UAS transgenes in outer, migratory border cells just prior to their migration, to express Src-CA and Src-WT. We used *c306*-Gal4 to drive *cskRNAi* expression earlier in development for the RNAi to have time to take effect (see Materials and methods). In control, UAS-lacZ-expressing egg chambers, the border cell cluster detaches from the anterior pole (Fig. 1 C) and migrates between the nurse cells (Fig. 1 D), reaching the oocyte by stage 10 (Fig. 1 E). Polar cells and their nuclei are smaller than those of the outer, migratory cells, and Fasciclin III (FAS3) accumulates to high levels at the interface between the two polar cells (Fig. 1, F and F'; and Video 1). Border

cell clusters expressing Src-WT exhibited normal organization (Fig. 1, G and G'). In contrast, the expression of Src-CA in outer, migratory border cells caused a dramatic change in cell shape and cluster organization (Fig. 1, H–J'). Furthermore, rather than surrounding the polar cells (Fig. 1, F and F'), border cells engulfed part of a polar cell (Fig. 1, H and H'; and Video 2), an entire polar cell (Fig. 1, I and I'; and Video 3), or even both polar cells (Fig. 1, J and J'; and Video 4). Similar phenotypes were observed following *cskRNAi* expression (Fig. 1, K1–L2'). In contrast, overexpression or overactivation of a number of kinases other than Src did not cause border cells to engulf polar cells, indicating that this is a specific phenotype (Table S1).

To confirm that polar cells were inside of border cells, we added anti-FAS3 antibody, which recognizes an extracellular epitope, for 15 min before fixation and without permeabilizing the tissue (see Materials and methods). As expected, anti-FAS3 effectively labeled control polar cells in which the extracellular epitope is accessible (Fig. S1, A–A', white arrows). Anti-FAS3 did not label internalized polar cells in Src-CA-expressing clusters (Fig. S1, B–C2', orange arrows), consistent with the idea that the epitope was inaccessible. Hence, hyperactivation of Src in outer border cells is sufficient to drive them to engulf polar cells.

We quantified engulfment by counting the percentage of clusters with at least one-half of one polar cell nucleus inside of a border cell. The two Src-CA lines caused the strongest effect with 70% and 80% engulfment (Fig. 1 M). Knockdown of *csk* also caused strong effects (up to 50%) whereas Src-WT expression was the weakest (10%; Fig. 1 M). We conclude that Src hyperactivity in border cells is sufficient to cause them to engulf polar cells.

Src hyperactivity disrupts border cell morphology and cluster cohesion

In controls, cell–cell adhesion and coordinated movement prevent cluster splitting, favoring cluster cohesion. Expression of Src-CA and *csk* RNAi caused border cells to round up and separate from one another. We quantified the phenotype by measuring the circularity index of individual border cells using the fluorescence of a plasma membrane GFP, PHGFP. Border cells expressing Src-WT were slightly rounder than controls, while Src-CA and *cskRNAi* had more severe shape changes (Fig. 2 A). Additionally, different kinds of protrusions were observed when Src was overexpressed or hyperactivated (Fig. 2, B–F and Fig. S1, D–F). In control, lacZ-expressing clusters, broad protrusions (Fig. 2 B, white arrowhead) were mainly observed in the border cell located at the front of the cluster rather than the side or back cells (Fig. 2 B; and Fig. 1, F and F'). When Src-WT was overexpressed, border cells exhibited blebs (Fig. 2 C, blue arrowhead), other unusual protrusions (Fig. 2 C, red arrowhead), or no

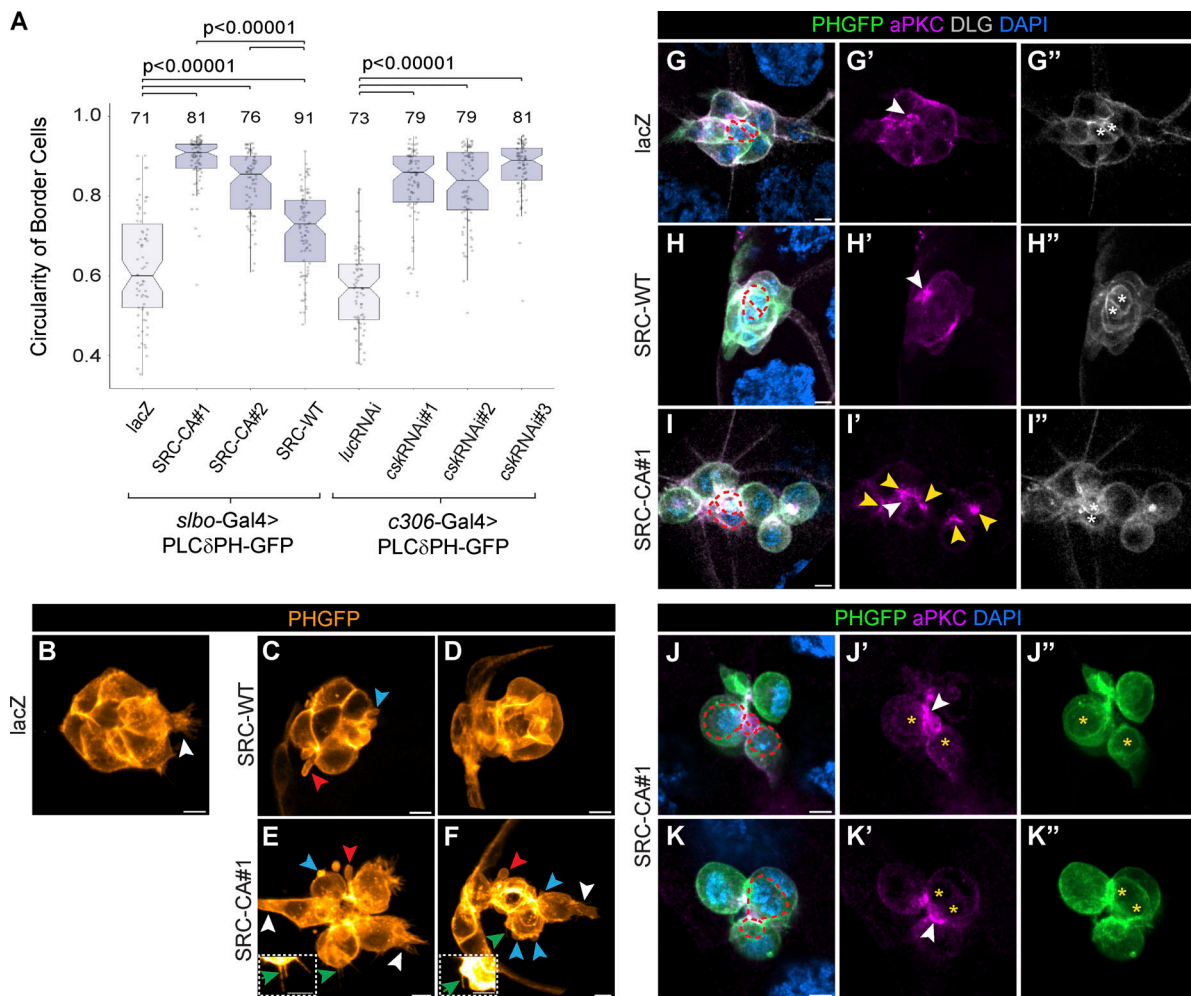


Figure 2. SRC hyperactivity disrupts border cell morphology and cluster cohesion. (A) Quantifications of the circularity index of individual border cells for the genotypes indicated. Box plots are used to represent the data. Each box plot shows the median (line) with 25th and 75th percentiles (hinges) plus $1.5 \times$ interquartile ranges (whiskers). Dots represent each cell analyzed, and the total number per genotype is indicated on the top of each box plot. Normal distribution was tested using Kolmogorov–Smirnov test. Since data were not normally distributed, a Mann–Whitney *U* test (one-tailed) was performed between controls and each experimental condition. P values are shown at the top of the graph. **(B–F)** Maximum intensity projection from eight slices (z-step: $0.5 \mu\text{m}$) of border cell clusters expressing UAS-PLC δ PHGFP and the genotypes indicated. White, blue, green, and red arrowheads point to lamellipodia, blebs, filipodia, and thick protrusions, respectively. Scale bar: $5 \mu\text{m}$. Insets in E and F correspond to a crop with increased intensity for PLC δ PHGFP from E and F images, allowing the observation of filipodia structures. Scale bar: $5 \mu\text{m}$. **(G–I')** Maximum intensity projection from 10 slices (z-step: $0.5 \mu\text{m}$) of border cell clusters expressing UAS-PLC δ PHGFP and the genotypes indicated. Egg chambers were stained with aPKC (magenta) and DLG (gray). DNA was visualized by DAPI (blue). Anterior pole of the cluster exhibited in G–G'' is pointing to the right. White or yellow arrowheads in G'–I' point to the apical domain (apical cap) of the polar cells or border cells enriched with aPKC. White asterisks in G''–I'' indicate non-internalized polar cells. Scale bar: $5 \mu\text{m}$. **(J–K'')** Maximum intensity projection from four slices (z-step: $0.4 \mu\text{m}$) of border cell clusters expressing UAS-PLC δ PHGFP and UAS-SRC-CA#1. Egg chambers were stained with aPKC (magenta). DNA was visualized by DAPI (blue). Yellow asterisks in J', J'', K', and K'' indicate partially internalized polar cells. White arrowheads in J' and K' point to the apical domain of the polar cells enriched with aPKC. Scale bar: $5 \mu\text{m}$. Polar cells in G–I, J, and K are outlined with a red dashed line.

protrusions (Fig. 2 D). However, Src-WT-overexpressing cells did not form normal leading protrusions, and the clusters exhibited random rather than directional motility (Video 5). Expression of Src-CA and *cskRNAi* generated all the protrusion types seen in Src-WT (Fig. 2, E and F; and Fig. S1, D and E), as well as thinner, filipodia-like protrusions (Fig. 2, E and F; and Fig. S1, E and F, green arrowheads), and normal lead-cell-like protrusions (Fig. 2, E and F, white arrowheads). All protrusions were observed in border cells independent of their position in the cluster. In contrast to Src-WT overexpression, Src-CA-expressing clusters migrated, albeit in a highly abnormal fashion (Fig. S1 G).

To determine whether roundborder cells had lost epithelial polarity, we assessed the subcellular localization of apical and basolateral markers such as aPKC and DLG proteins. In control clusters, border cells maintain a shared apicobasal polarity such that the apical marker aPKC is enriched at apical border cell/border cell, border cell/polar cell, and polar cell/polar cell junctions, and basolateral proteins like DLG accumulate in a complementary pattern (Fig. 2, G–G''). Polar cells can be recognized by their distinctively small, constricted apical “caps” (Fig. 2, G and G', arrowhead). Src-WT-expressing clusters showed relatively normal polarity, including the recognizable

apical cap (Fig. 2, H-H', arrowhead). Interestingly, in Src-CA-expressing clusters, each individual cell maintained localization of aPKC and DLG (Fig. 2, I-I', yellow arrowheads for border cells and white arrowheads for polar cells). However, the cohesion of border cell clusters was disrupted and the coordination of individual polarities into a collective polarity was lost (Fig. 2, I-I'). The apical domain of polar cells was the last to be internalized, suggesting that engulfment is initiated basally (Fig. 2, J-K'). Egg chambers with border cells migrating individually or in groups of two to three cells (split cluster category, see Materials and methods) were frequently observed in Src-CA expression or *csk* downregulation but were never present in Src-WT-expressing or control clusters (Fig. S1 G). These findings suggest that Src activity must be controlled in border cells to preserve their morphology, cluster organization, and directional migration.

Hyperactive Src also causes posterior polar cell internalization

We next asked if the ability of hyperactive Src to cause polar cell internalization could occur in non-migratory cells. We took advantage of the natural architecture of the egg chambers since another polar cell pair is present at the posterior pole (Fig. S1 H) surrounded by follicle cells (FCs) that do not migrate (Fig. S1, I and I'). We quantified polar cell internalization at the posterior poles of control egg chambers and those expressing Src-CA at stage 10 of oogenesis. Similar to the anterior pole, hyperactive Src was sufficient to drive posterior FCs engulfment of one (Fig. S1, J and J') or both polar cells (Fig. S1, K and K'). However, polar cell internalization frequency was lower (21%; Fig. S1 L), possibly as a consequence of the later onset of *slboGal4* expression at the posterior. Src-CA-expressing clusters that never detached from the anterior pole of egg chambers were also able to internalize polar cells (Fig. S1, B-B' and C1-C2'). Thus, cell migration is not a prerequisite for polar cell internalization.

Internalized polar cells remain alive

In the early stages of oogenesis, more than two polar cells initially develop, and the excess cells are eliminated by apoptosis (Khammari et al., 2011). In this context, the nearby epithelial follicle cells engulf and digest dying polar cells (Torres et al., 2017). To test whether border cells expressing Src-CA engulf living or dead polar cells, we checked for the cleaved and activated form of the apoptotic marker Death Caspase-1 (DCP1). DCP1 is an effector caspase, the cleavage of which indicates that apoptosis is underway (Song et al., 1997). As a positive control, we expressed the pro-apoptotic gene *reaper* under the control of *slbo-Gal4*. *Reaper*-expressing cells exhibited signs of death, including pyknotic nuclei (Fig. 3 A, arrows). Cleaved DCP1 (cDCP1) was detected only in dying cells, as expected (Fig. 3, A and A'). In control clusters expressing *lacZ*, no cDCP1 was detected, and all nuclei looked healthy (Fig. 3, B and B'). Upon expression of Src-CA, polar cells maintained normal nuclear morphology. Furthermore, neither polar cells that were completely inside of a border cell (Fig. 3, C and C', yellow asterisk) nor un-engulfed polar cells (Fig. 3, C and C', white asterisk) expressed cDCP1. We conclude that polar cells were not undergoing caspase-dependent cell death either before or after their engulfment.

Another form of cell death relies on acidification by lysosomal enzymes. For example, Mondragon et al., (2019) showed that during stages 12 and 13 of normal *Drosophila* oogenesis, anterior stretch FCs release lysosomal enzymes to kill the nurse cells. They used LysoTracker dye to detect the presence of acidic compartments, the upregulation of which is an indicator of lysosome-mediated cell death. To determine whether polar cells were dying through lysosomal cell death, we compared LysoTracker staining of Src-CA-expressing egg chambers to *lacZ* controls. In control flies, there are rare examples of sporadic egg chamber death, which were positive for LysoTracker and served as a positive control for the staining (Fig. 3, D and D'). In both controls and Src-CA border cell clusters, we could detect acidic organelles, presumably lysosomes (Fig. 3, E-F'). However, no elevation of LysoTracker staining was observed in polar cells in *lacZ*- (Fig. 3, E and E') or Src-CA-expressing border cell clusters, even when polar cells were engulfed (Fig. 3, F and F'). There was no upregulation of acidic compartments in the cytoplasm of engulfing border cells that expressed Src-CA. These results suggest that internalized polar cells were not being digested by border cells with elevated Src activity.

Since polar cells are engulfed but not degraded, we investigated at which stage engulfment is arrested. The small GTPase Rab5 is normally transiently associated with early phagosomes while Rab7 is recruited later (Desjardins et al., 1994; Vieira et al., 2003). Rab5 and Rab7 were expressed at higher levels in Src-CA than in control (Fig. 3, G-L'), but only Rab7 was enriched on engulfed polar cells (Fig. 3, K-L'), suggesting that phagocytosis arrests right before lysosomal degradation. In addition, the autophagy marker Atg8 (Jipa et al., 2021; Takáts et al., 2013) was clearly visible in dying egg chambers as previously described (Nezis et al., 2010; Fig. 3, M and M') but was absent from control and engulfed polar cells (Fig. 3, N-O').

To follow the dynamics of engulfment, we conducted real-time imaging on egg chambers expressing Src-CA compared with control clusters. The expression of UAS-PLC δ PHGFP allowed us to identify and follow border cell membranes, and we used DAPI to label cell nuclei. Control border cell clusters were tracked during detachment from the anterior pole and forward migration between the nurse cells ($n = 3$; Video 6). Polar cells were always located in the center of the cluster surrounded by ovoid and migratory border cells (Fig. S1, M1-M3). When Src-CA was expressed, border cells were unusually dynamic in the dorsoventral axis ($n = 6$; Video 7). Polar cells were observed partially (Fig. S1 N1, orange asterisk) and fully internalized by border cells (Fig. S1, N2 and N3, yellow asterisk). Once polar cells were completely engulfed, we never saw them escape (Fig. S1, N2, N3, and O1-O3'). We estimate that completion of polar cell engulfment takes 10–20 min ($n = 4$).

To investigate the fates of internalized polar cells, we followed border cells for 1 or 2 h after engulfment. Remarkably, border cells containing polar cells retained the ability to migrate and the nuclei of engulfed polar cells maintained a healthy appearance (Fig. S1, O1-O3' and Video 8). Elevated Src activity compromised egg chamber survival, preventing us from tracking internalized cells for longer periods of time. Additionally, in fixed samples, most post-stage-10 egg chambers died (Fig. S1 P,

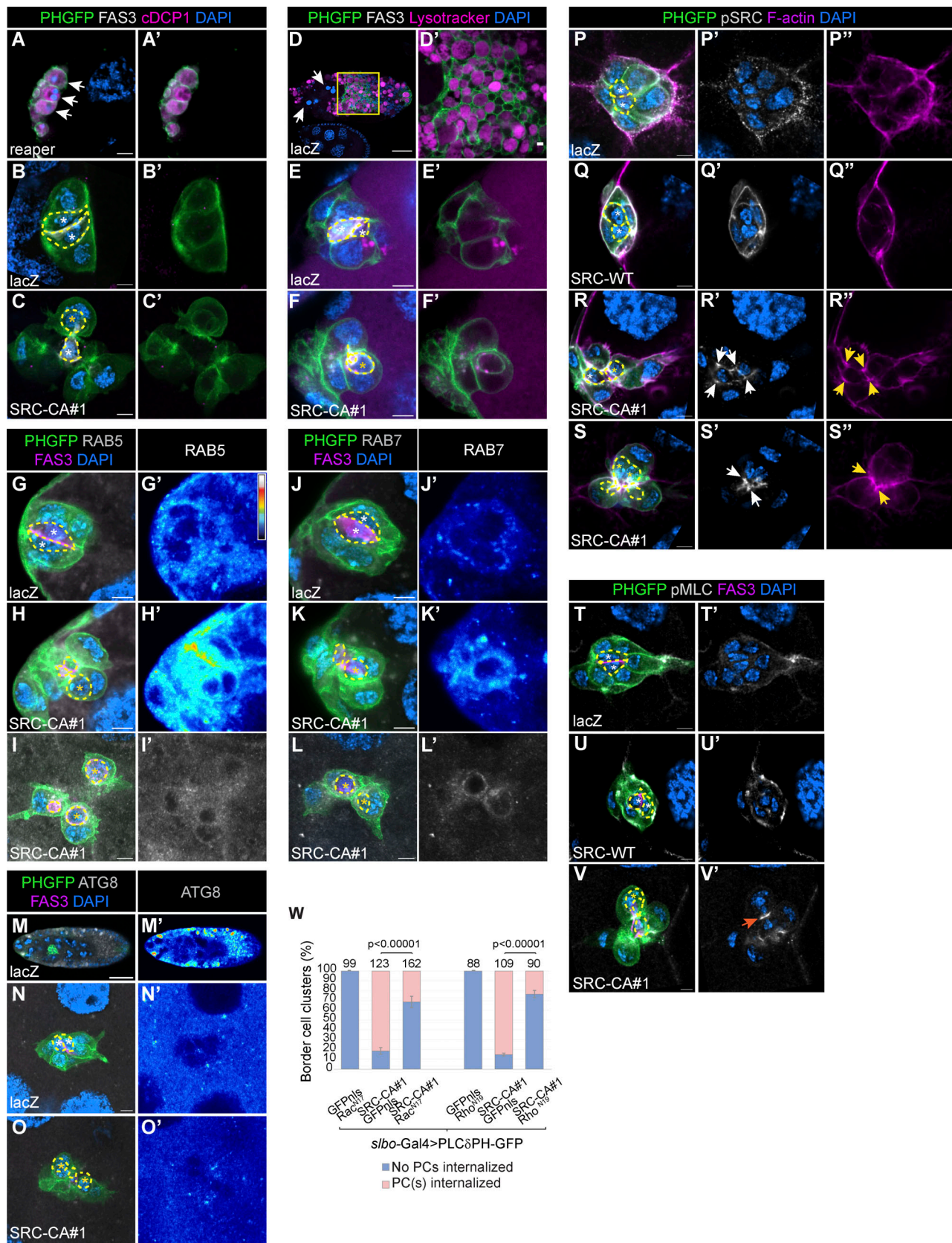


Figure 3. **Internalized polar cells do not exhibit signs of death, and their engulfment depends on Rac and Rho.** (A–C') Single sections from confocal images of border cell clusters from stage 10 egg chambers expressing UAS-PLCδPHGFP and the genotypes indicated. Egg chambers were stained with FAS3 (gray), cDCP1 (magenta), and DNA was visualized by DAPI (blue). Arrows in A indicate pyknotic nuclei. White asterisks in B and C indicate non-internalized polar

cells, and yellow asterisk in C indicates internalized polar cell. Scale bar: 5 μm . **(D–F)** Single sections from confocal images of a dying egg chamber (D and D') or of border cell clusters from egg chambers in stage 10 (E–F'), expressing UAS-PLC δ PHGFP and the genotypes indicated. Egg chambers were stained with FAS3 (gray), LysoTracker dye (magenta) to visualize acidic compartments, and DAPI (blue) to visualize DNA. White arrows in D point to pyknotic nurse cell nuclei. Yellow inset in D is shown in a higher magnification in D'. White asterisks in E indicate non-internalized polar cells, and yellow asterisk in F indicates internalized polar cells. Scale bar is 50 μm for the egg chamber in D and 5 μm for D' and for border cell clusters in E–F'. **(G–L)** Maximum intensity projection from five slices (G–I') or nine slices (J–L'; z-step: 0.5 μm for G–H' and J–K', 0.16 μm for I, I', L, and L') of border cell clusters expressing UAS-PLC δ PHGFP and the genotypes indicated. Images in I, I', L, and L' were obtained by airyscan imaging to visualize the localization of RAB5 (I and I') and RAB7 (L and L') at a high spatial resolution, and are not suitable for comparison of expression levels. Egg chambers were stained for FAS3 (magenta) and for RAB5 (G–I) or RAB7 (J–L; gray). DNA was visualized by DAPI (blue). White asterisks in G and J indicate non-internalized polar cells and yellow asterisks in H–I and K and L indicate internalized polar cells. Scale bar: 5 μm . **(G'–L')** Images from G–L showing only RAB5 (G'–I') or RAB7 (J'–L') staining in Royal LUT where white represents the highest amount of the indicated protein and black the lowest one. **(M–O)** Single section (M) or maximum intensity projection from six slides (N and O; z-step: 0.5 μm) of a dying egg chamber (M) or border cell clusters expressing UAS-PLC δ PHGFP and the genotypes indicated. Egg chambers were stained for FAS3 (magenta) and ATG8 (gray). DNA was visualized by DAPI (blue). Scale bar is 50 μm for the egg chamber in M and 5 μm for border cell clusters in N and O. **(M'–O')** Images from M–O showing only ATG8 staining in Royal LUT. **(P–S')** Single sections from confocal images of border cell clusters from egg chambers at stage 9 or 10 expressing UAS-PLC δ PHGFP and the genotypes indicated. Egg chambers were stained with pSrc (gray), F-actin (magenta), and DAPI (blue). White asterisks in P–R indicate non-internalized polar cells. In R, one polar cell is being internalized (yellow asterisk) by one border cell, and in S both polar cells are being internalized (yellow asterisks) by one border cell. White arrows in R' and S point to pSrc accumulation and yellow arrows in R'' and S'' point to F-actin accumulation. Scale bar: 5 μm . **(T–V')** Single sections from confocal images of border cell clusters from egg chambers at stage 9 or 10 expressing UAS-PLC δ PHGFP and the genotypes indicated. Egg chambers were stained with pMLC (gray), FAS3 (magenta), and DAPI (blue). White asterisks in T and U indicate non-internalized polar cells and the yellow asterisk in V indicates an internalized polar cell. The orange arrow in V' points pMLC accumulation along with the squeezing of a polar cell nucleus. Scale bar: 5 μm . **(W)** Quantifications of polar cell internalization events from stage 10 egg chambers of the indicated genotypes. Error bars: mean \pm SEM ($n = 3$). The total number of clusters analyzed (n) is indicated at the top of each bar. Statistical significance was assessed with a Fisher exact test (one-tailed) and P values are shown at the top of the graph. Polar cells in B, C, E, L, and N–V are outlined with a yellow dashed line.

orange asterisks, Fig. S1, Q and R). The few egg chambers that survived presented a variety of developmental defects. Surprisingly, we could observe border cells with internalized polar cells in those few post-stage-10 egg chambers (Fig. S1, S and S'). Considering that polar cell internalization occurred early in stage 9, which takes ~ 6 h, we infer that internalized polar cells can remain alive for at least 9 h.

Src-dependent polar cell internalization requires actin, myosin, Rac, and Rho

To investigate whether elevated Src activity led to polar cell internalization through the phagocytic machinery, we examined actin and myosin, which are the principal effectors of phagocytosis. We assessed the subcellular localization of active Src, F-actin, and the active form of myosin in clusters expressing Src-CA compared with clusters expressing Src-WT or the control, lacZ. We used the pSrc antibody which recognizes phosphorylation of the activating tyrosine in the catalytic domain, phalloidin, to label filamentous actin (F-actin), and an antibody against phospho-Myosin Light Chain 2 (pMLC).

In control clusters, pSrc appeared in dispersed puncta and accumulated primarily at the periphery of the cluster where border cells contact nurse cells (Fig. 3, P and P'). Overexpression of Src-WT caused pSrc to accumulate at all border cell membranes (Fig. 3, Q and Q'). Upon expression of Src-CA, pSrc accumulated at contacts between border cells and polar cells, regardless of whether polar cells were being internalized (Fig. 3, R–S', yellow asterisks) or not (Fig. 3, R and R', white asterisk). Expression of Src-CA, Src-WT, and RNAi of *csk* led to a statistically significant increase in Src activity compared with their respective controls (Fig. S2 A). F-actin colocalized with pSrc (Fig. 3, P''–S'') and active myosin accumulated at points of constriction (Fig. 3, T–V', orange arrow). Src-CA and Src-WT had similar effects on overall pSrc levels, suggesting that it is the localization of pSrc rather than the level of activation that

explains the differences in phenotype. In the few instances where Src-WT caused polar cell internalization, we also observed the accumulation of pSrc and F-actin at the sites of engulfment (Fig. S2, B–C').

F-actin and Myosin accumulate in phagocytic cups downstream of the small GTPases Rac and Rho (Mao and Finnemann, 2015). So, we tested whether downregulating Rac and/or Rho activity would suppress the Src-CA-induced engulfment phenotype. We expressed the dominant negative forms of Rac1 (Rac1^{N17}; Luo et al., 1994) and Rho1 (Rho1^{N19}; Barrett et al., 1997). When they were individually coexpressed with GFPnls (see Materials and methods), no polar cell internalization phenotype was observed (Fig. 3 W), but border cell migration was fully blocked (Fig. S2 D). Coexpression of Rac1^{N17} with Src-CA reduced polar cell internalization from $\sim 84\%$ to 32%, and Rho1^{N19} reduced it to 24% (Fig. 3 W). This rescue shows that cells with elevated Src activity require Rac and Rho to complete engulfment.

SHARK and FAK kinases function downstream of Src in polar cell internalization

SHARK (and its mammalian counterpart SYK and ZAP70 kinases) and FAK are non-receptor tyrosine kinases phosphorylated and activated by SFKs in many biological processes including phagocytosis (Finnemann, 2003; Metheniti et al., 2001; Scheib et al., 2012; van Oers et al., 1996; Wu et al., 2009; Ziegenfuss et al., 2008). To examine the effect of Src on these two kinases, we used antibodies that recognize the tyrosine residues phosphorylated by Src (SHARK-Y927 [pSHARK] (Biswas et al., 2006) and FAK-Y397 [pFAK]) and compared egg chambers expressing Src-CA, Src-WT, or lac-Z (Fig. 4, A–H). Although Src-CA generated a fourfold increase in pSHARK and Src-WT caused a 2.5-fold increase (Fig. 4 D), only Src-CA led to a significant increase in pFAK (Fig. 4 H). Remarkably, when Src-CA was expressed, pSHARK and pFAK accumulated at border cell–polar cell

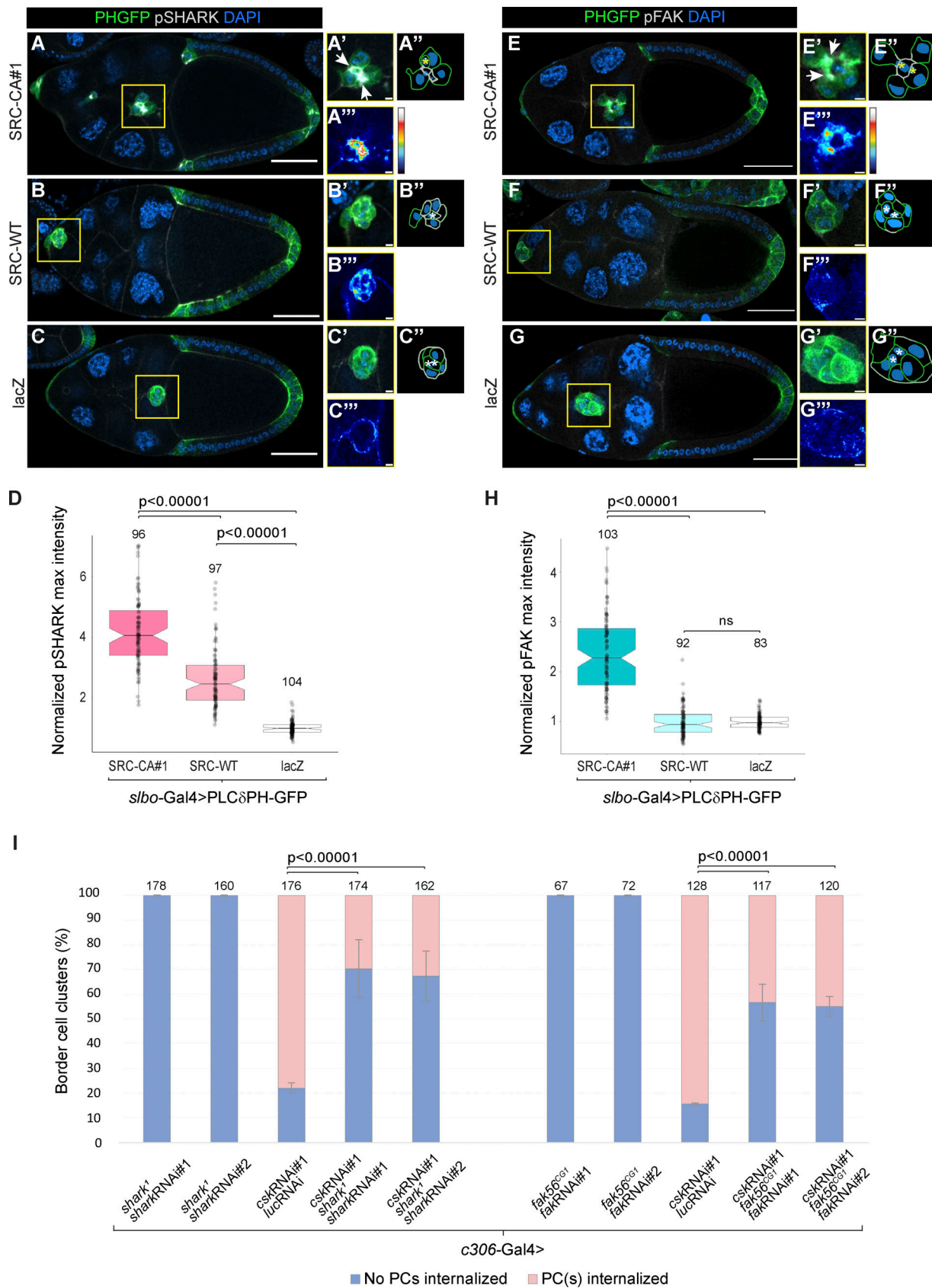


Figure 4. **SHARK and FAK kinases function downstream of SRC in polar cell internalization.** (A–G) Single sections from confocal images of egg chambers at stage 10 expressing UAS-PLCδPHGFP and the genotypes indicated. In A–C, egg chambers were stained with SHARK-Y927 (pSHARK; gray), and in E–G, egg chambers were stained with FAK-Y397 (pFAK; gray). DAPI (blue) was used to visualize DNA. Scale bar is 50 μm. Yellow insets frame border cell clusters, and

their respective crop images are shown in A'–G'. (**A''–G''**) Schematic representations of the images shown in A'–G'. White or yellow asterisks indicate non-internalized or partially internalized polar cells, respectively. (**A'''–G'''**) Same images are shown in A'–G', where pSHARK (A'''–C''') or pFAK (E'''–G''') are shown in Royal LUT, where white represents the highest amount of the protein and black the lowest one. Scale bar is 5 μ m. (**D–H**) Quantifications of normalized pSHARK (D) or pFAK (H) maximal intensity (see Materials and methods) from stage 9 or 10 egg chambers of the indicated genotypes. Box plots are used to represent the data. Each box plot shows the median (line) with 25th and 75th percentiles (hinges) plus 1.5 \times interquartile ranges (whiskers). Dots represent each cluster analyzed and their total number per genotype (*n*) is indicated on the top of each box plot. Normal distribution was tested using Kolmogorov–Smirnov test. Since data were normally distributed, an ANOVA test (one-tailed) with post-hoc Tukey was performed to evaluate statistical significance. P values are shown at the top of the graph. ns indicates not significant. (**I**) Quantifications of polar cells internalization from egg chambers at stage 10 of the indicated genotypes (see Materials and methods). Error bars: mean \pm SEM (*n* = 3). The total number of clusters analyzed (*n*) is indicated at the top of each bar. Statistical significance was assessed with a Fisher exact test (one-tailed) and P values are shown at the top of the graph.

contacts (Fig. 4, A'–A''' and E'–E'''), like pSrc, F-actin, and Myosin (Fig. 3, R–S'', V, and V').

We performed epistasis tests to determine if SHARK and/or FAK were required to promote polar cell internalization. To reduce SHARK or FAK expression, amorphic alleles of *shark* (*shark¹*) or *fak* (*fak56^{CG1}*) were used along with two different RNAi lines for *shark* (*sharkRNAi#1* or *sharkRNAi#2*) or for *fak* (*fakRNAi#1* or *fakRNAi#2*). To increase Src activity, we downregulated *csk* by RNAi (*cskRNAi#1*) and coexpressed it with *luciferaseRNAi* (*lucRNAi*) to control for the number of UAS transgenes. Downregulation of *csk* led to polar cell internalization in ~81% of egg chambers examined (Fig. 4 I) and ~40% migration failure (Fig. S2 E). Reduction of SHARK or FAK alone generated neither polar cell internalization nor border cell migration defects. However, simultaneous expression of *cskRNAi#1* and downregulation of *shark* led to a reduction of polar cell internalization to ~32%, with *fak* downregulation to ~44% (Fig. 4 I) as well as a rescue of border cell migration defects to ~7% and ~22%, respectively (Fig. S2 E). Interestingly, cell and cluster morphology were also rescued when *shark* or *fak* were downregulated in *cskRNAi*-expressing cells (Fig. S2, F–H'). Together, these results suggest that SHARK and FAK proteins function downstream of Src not only for polar cell internalization but also for abnormal migration and cell and cluster morphology.

Src-dependent polar cell internalization requires integrins but not Draper

The classical and most studied phagocytic receptors have an immunoreceptor tyrosine-based activation motif (ITAM) region in their intracellular domain, which is phosphorylated by SFKs upon ligand–receptor interaction, allowing for the recruitment of SYK kinases and triggering of engulfment (Uribe-Querol and Rosales, 2020). In *Drosophila*, the ITAM receptor Draper (Drpr) is required for follicle cells to recognize the germline during engulfment of late-stage nurse cells or in nutrient-deprived conditions (MacDonald et al., 2006; Serizier et al., 2022; Timmons et al., 2017). To test whether Src-CA-expressing border cells require Drpr for polar cell internalization, we expressed Src-CA in a *drpr* null mutant background. Unexpectedly, mutating *drpr* did not alter the internalization of polar cells by SrcCA-expressing border cells (Fig. 5 A).

Integrins are heterodimeric (α and β subunit) receptors that also promote mammalian and *Drosophila* phagocytosis (Finnemann, 2003; Finnemann et al., 2007; Meehan et al., 2015; Nonaka et al., 2013; Sun et al., 2021; Torres-Gomez et al., 2020).

Therefore, we tested genetic interactions between Src and integrin. Reduction of the integrin β_{PS} subunit by itself did not

cause defects in border cell migration, as previously reported (Llense and Martín-Blanco, 2008) and did not lead to polar cell internalization (Fig. 5 A). In contrast, downregulating the integrin β_{PS} subunit fully rescued the polar cell engulfment caused by *cskRNAi* (Fig. 5 A). Polymerase chain reaction amplification with specific primers confirmed the presence of the inverted repeated sequence of *csk* RNAi line in the flies, validating this result (Fig. S3 A). Similarly, partial loss of function of *mys*, the gene encoding the integrin β_{PS} subunit, rescued border cell migration (Fig. S3 B, *cskRNAi* = 50% complete migration; *cskRNAi*, *mys¹*, *mysRNAi* = 85% complete migration) and cell and cluster morphology defects generated by *csk* RNAi (Fig. S3, C and D).

To determine the subcellular localization of β_{PS} when Src was hyperactivated or overexpressed, we used an antibody specific for this subunit (Brower et al., 1984; Llense and Martín-Blanco, 2008). Compared with control clusters, Src-WT or Src-CA expression increased the β_{PS} signal. In addition, β_{PS} was enriched at contact site(s) between border cells and polar cells during engulfment (Fig. 5, B–D''). These results suggest that elevated Src activity is upstream of the integrin receptor and interacts with the β_{PS} subunit to drive both polar cell internalization and abnormal cell migration and morphology.

Drpr-Src-Shark is a conserved signaling pathway for *Drosophila* phagocytosis. Since we found that Drpr was not required for Src-driven polar cell internalization, we asked whether Shark is still activated by Src in the absence of *drpr*. To test this, we used pSHARK antibody to stain egg chambers expressing Src-CA alone or in a *drpr* mutant context. Notably, the absence of *drpr* did not affect pSHARK levels when Src was highly increased, suggesting that Src activation of SHARK is Drpr-independent (Fig. S3, E–F''). In contrast, concomitant reduction of *csk* and *mys* expression prevented pSHARK accumulation at border cell–polar cell contact sites (Fig. S3, G–H''), indicating that Src can only phosphorylate and activate SHARK in the presence of integrin receptors. Together, our results support a model in which high and localized Src activity causes abnormal localization of integrin receptors to border cell/polar cell contacts leading to activation of FAK, SHARK, Rac, and Rho; recruitment of actomyosin; and ultimately to polar cell cannibalism.

Discussion

Hyperactivated Src is sufficient to drive live cell engulfment

SRC-family kinases are necessary for phagocytosis in cells as diverse as mammalian innate immune cells (Lowell, 2011; Wetzel et al., 2016), *Drosophila* glia (MacDonald et al., 2006), and

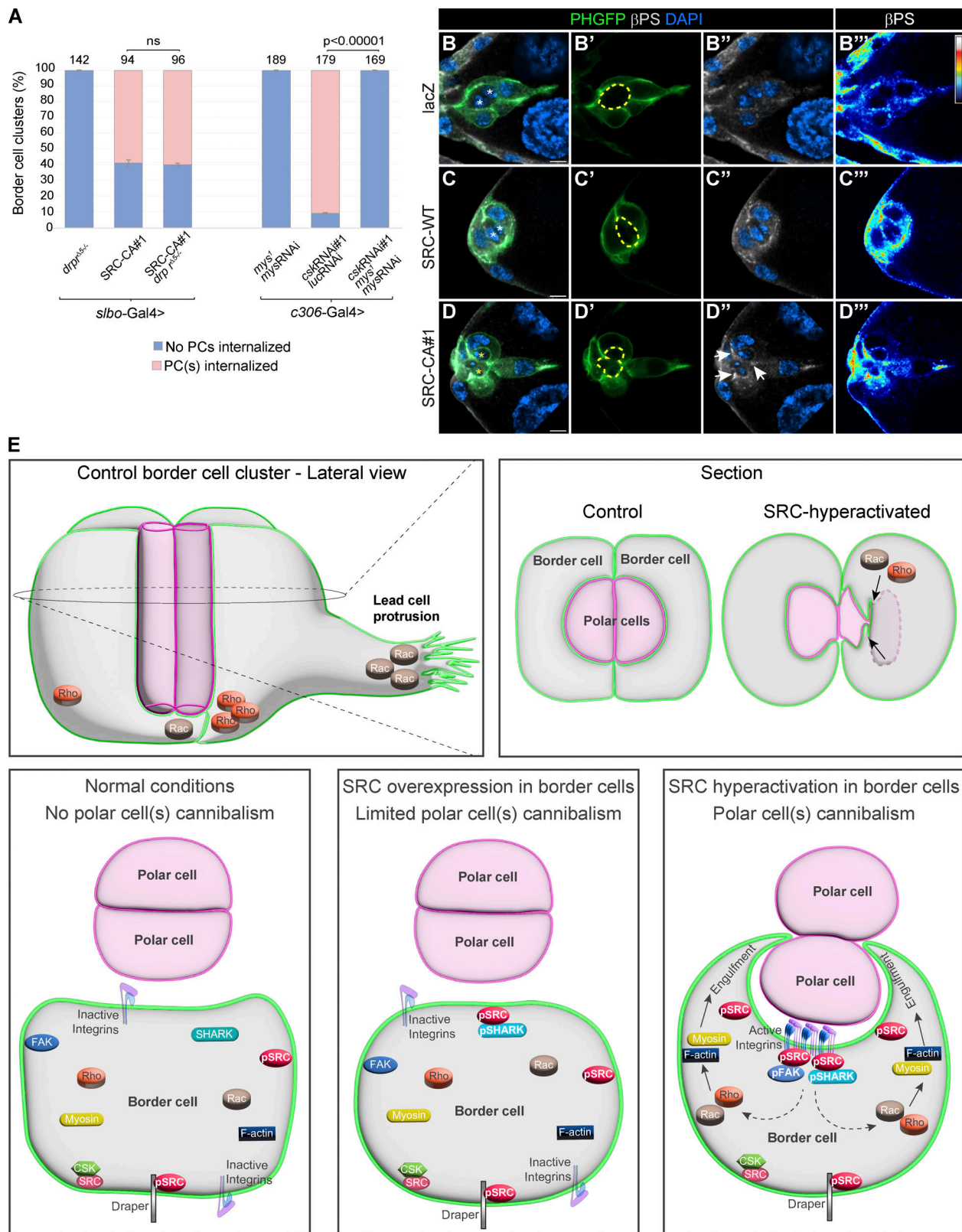


Figure 5. **SRC-dependent polar cell internalization requires integrins but not Draper.** (A) Quantifications of polar cell internalization from egg chambers at stage 10 for the indicated genotypes (see Materials and methods). Error bars: mean \pm SEM ($n = 3$). The total number of clusters analyzed (n) is indicated at the top of each bar. Statistical significance was assessed with a Fisher exact test (one-tailed) and P values are shown at the top of the graph. ns indicates not significant. (B–D''') Single section from confocal images of border cell clusters from egg chambers at stage 9 expressing UAS-PLC δ PHGF (green) and the genotypes indicated. Egg chambers were stained with β PS (gray) and DAPI (blue). White or yellow asterisks indicate non-internalized or partially internalized polar cells, respectively. White arrows in D'' point to the accumulation of β PS at the contact site(s) between border cell–polar cell. Images in B'''–D''' indicate

βPS staining in a Royal LUT, where white represents the highest amount of the protein and black the lowest one. Scale bar: 5 μm. Polar cells are outlined with a yellow dashed line in B'–D'. **(E)** Model of normal or elevated SRC activity in border cells. Top panels: In control border cell clusters, Rac activity is high in the lead cell protrusion and at the front of follower cells. Rho activity is localized posteriorly. When SRC is hyperactivated, it leads to the enrichment of Rac and Rho at the site of engulfment. Bottom panels: For clarity, only one border cell of the cluster is represented. Left: Wild-type border cells have normal levels of SRC activity. In this condition, cells are ovoid and no cannibalism of polar cells is observed. Most SRC is negatively regulated by CSK, but an active pool of the protein can phosphorylate Draper receptor or other targets, ensuring normal behavior. Integrin receptors remain inactive. Middle: SRC overexpression in border cells leads to a semicircular shape and limited polar cell cannibalism. Elevated SRC activity is sufficient to slightly increase pSHARK, but it is not enough to activate and recruit pFAK at border cell–polar cell contacts. Right: Hyperactivation of SRC causes border cells' rounding and localized accumulation of active SRC at border cell–polar cell contacts. Localized SRC activity promotes the relocalization of Integrin receptors at the site of engulfment. FAK and SHARK tyrosine kinases are also activated and recruited by SRC to those contact sites. All these activated proteins serve as a node of signal amplification, triggering cannibalism of polar cells through the activation of Rac and Rho GTPases, F-actin, and Myosin. Dashed arrows represent a direct or indirect interaction.

ovarian follicle cells (Serizier et al., 2022; Timmons et al., 2017). Here, we show that the expression of hyperactivated Src or downregulation of the negative regulator of Src activity is sufficient to drive the heterotypic engulfment of polar cells by border cells. It is interesting that we did not observe border cells engulfing each other or other follicle cells. Polar cells are intimately connected to border cells and are smaller than border cells, and it is possible that this facilitates their engulfment. Additionally, polar cells express high levels of E-cadherin on their surfaces (Niewiadomska et al., 1999), which may further enhance their susceptibility to engulfment (Overholtzer et al., 2007; Sun et al., 2014).

Whereas wild-type border cells carry polar cells as they migrate from the anterior end of the egg chamber to the developing egg, border cells expressing SrcCA or *cskRNAi* engulf them. One border cell can engulf a part of a polar cell, a whole polar cell, or even two whole polar cells. Individual SrcCA-expressing border cells appear to compete for the polar cells, sometimes tearing them into pieces.

Importantly, we show that engulfment is initiated and carried out by the cells that express hyperactive Src, the border cells, rather than the engulfed polar cells. Therefore, despite the enrichment in E-cadherin, typical of entosis (Overholtzer et al., 2007), the process that Src is activating is not entosis because entosis by definition is initiated by the cell that is eventually internalized (Borensztein et al., 2021; Yang and Li, 2012). The observed Src-mediated engulfment meets the definition of cannibalism, where one cell persists (living or dead) inside another (Brown et al., 2015).

The mechanism by which hyperactivated Src drives polar cell engulfment requires multiple components that follicle cells normally use to engulf and eliminate germline cells. Although border cells do not normally engulf polar cells, follicle cells do engulf nurse cells late in egg chamber development: after nurse cells transfer the bulk of their cytoplasm to the oocyte, anterior follicle cells kill and engulf nurse cells. Additionally, when females are protein-deprived, the germline dies at stage 8 and follicle cells engulf the dying germline to recoup the nutrients and support the female fly's survival. These engulfment events require Src and SHARK. These normal engulfment behaviors also require both Drpr and integrin receptors, which also promote phagocytic activity in the glia (Ziegenfuss et al., 2008). We found that hyperactive Src kinase strictly requires integrin but not Drpr, suggesting that Src-CA bypasses the requirement for Drpr but not integrin. Integrins are adhesion receptors that can be activated by ligand binding or by “inside out” signaling (Kim

et al., 2011; Springer and Dustin, 2012). Our data support the idea that hyperactive Src activates inside out integrin signaling.

Border cells with hyperactivated Src also require FAK, SHARK, Rho, and Rac activities to execute polar cell engulfment (Fig. 5 E). Strikingly though, border cells do not kill or eliminate polar cells and can even migrate, albeit abnormally, carrying along the internalized cells. This suggests that Src is sufficient to activate only part of the pathway and perhaps Drpr signaling is critical for killing engulfed targets (Etchegaray et al., 2012).

Src localization and activity drive cell engulfment

In the present work, we use three different ways to modulate Src expression and activity: we overexpressed the wild-type protein (Src-WT), expressed a constitutively active form of Src (Src-CA), and knocked down the Src inhibitory kinase Csk (*cskRNAi*). Src-CA and *cskRNAi* caused more engulfment than Src-WT. This is consistent with the qualitative differences observed between hyperactive Src and Src-WT. For instance, hyperactive Src causes a higher frequency of epidermal hyperplasia than Src-WT in mice (Matsumoto et al., 2003), and Src-WT overexpression is insufficient to induce transformation (Lipsick, 2019). Surprisingly, we found that Src-WT and Src-CA induced similar levels of fully active pSrc (phosphorylated in the kinase domain at Tyr419; Roskoski et al., 2015). In contrast, *cskRNAi* only induced a modest increase. This suggests that the global level of pSRC is not the critical determinant of cell behavior. Importantly, we observed local enrichment of pSrc at sites of polar cell engulfment, suggesting that it might be the site of activity—rather than the global level of active Src—that determines the frequency of engulfment. We also show that homogeneous pSrc enrichment at the cell membrane in Src-WT is not compatible with the formation of productive protrusions that are required for directional cell migration. FRAP studies have also shown that the open conformation of constitutively active SRC (corresponding to Src-CA and *cskRNAi*) promotes its association with membrane-associated proteins, while SRC-WT associates with the membrane through lipid interactions (Shvartsman et al., 2007). Therefore, differences in interaction partners or an increased residence time of pSrc in specific membrane subdomains might explain the phenotypic differences we observed.

Src-driven cell-in-cell structures could drive tumor growth and dissemination

SRC is known to promote tumor growth and metastasis, is overactivated in a variety of human cancers, and is associated

with poor prognosis (Irby and Yeatman, 2000). Our findings show that high, localized levels of active Src can promote cell cannibalism. The ability to engulf neighboring cells might provide fuel to rapidly divide cancer cells in nutrient-limiting conditions. Engulfment of normal cells by tumor cells may also cause tissue damage as tumors grow. In addition, our observation that at least some cells can survive inside other cells suggests that Src-mediated cannibalism may also contribute to shielding tumor cells and promote drug resistance and cancer recurrence (Gutwillig et al., 2022; Mlynarczuk-Bialy et al., 2020). In addition, Src hyperactivation promotes abnormal migration. Therefore, cancer cells inside cancer cells could not only be protected from immune clearance but might even migrate to distant sites. These results suggest multiple new ideas for how hyperactivated Src might contribute to poor patient prognosis.

Materials and methods

Drosophila stocks and genetics

The following fly lines were obtained from the Bloomington *Drosophila* Stock Center: UAS-PLC δ PHGFP (chr. III; 39693), UAS-lacZ (chr. III; 3956), UAS-Src-CA#2 (chr. III; 6410), UAS-GFPnls (chr. II; 4775), UAS-GFPnls (chr. III; 4776), UAS-Rho1^{N19} (chr. X; 7327), *c306-Gal4* (chr. X; BL3743), UAS-luciferase-RNAi (chr. III; 31603), UAS-*csk*-RNAi#3 (chr. III; 35174), UAS-*shark*-RNAi#1 (chr. III; 55874), UAS-*shark*-RNAi#2 (chr. III; 25788), UAS-*fak*-RNAi#1 (chr. III; 33617), UAS-*fak*-RNAi#1 (chr. III; 29323), *w¹¹¹⁸* (chr. X; 3605), and *mys¹* (chr. X; 59). Strains carrying RNAi constructs from VDRC collections were UAS-*csk*-RNAi#1 (chr. II; 109813), UAS-*csk*-RNAi#2 (chr. III; 32877), and UAS-*mys*-RNAi (chr. II; 29619). Additional fly lines used include UAS-Src-CA#1 (chr. II) and UAS-Src-WT (chr. III) (Takahashi et al., 1996) (kindly provided by Dr. Kojima T Graduate School of Frontier Sciences, The University of Tokyo, Tokyo, Japan, *shark¹/CyO* (kindly provided by Prof. Berg C.A. University of Washington, Seattle, WA, USA), *fak56^{CGI}* (Ueda et al., 2008) (kindly provided by Prof. Palmer R, Institute of Biomedicine, Sahlgrenska Academy, University of Gothenburg, Gothenburg, Sweden), UAS-Fak56^{Y430F} (chr. III; kindly provided by Prof. C.F. Wu, University of Iowa, Iowa City, IA, USA), *drpr ^{Δ 5}* (kindly provided by Dr. Freeman MR, The Vollum Institute, Oregon Health & Science University, Portland, OR, USA), UAS-lambda-Otk and pUAS-Otk (II; from Dr. Goodman CS, W.G. (Bill) Hefner VA Medical Center, Salisbury, NC, USA). UAS-reaper, (chr. X), UAS-Rac1^{N17} (chr. III), UAS-lambda-Top4.4 (III), UAS-lambda-Top4.2 (X), and UAS-lambda-ROR and UAS-HopTum are from the Montell D.J stock. *c306-Gal4* (chr. X) and *slbo-Gal4* (chr. II; Montell D.J, stock) were used as drivers to target UAS constructions in border cell clusters. *c306-Gal4* is expressed in both border cells and polar cells from the end of the germarium while *slbo-Gal4* is expressed in border cells and posterior follicle cells from stage 9 as well as centripetal cells from stage 10. UAS-lacZ or UAS-*luc*-RNAi were used as controls of over-expression or gene downregulation, respectively, or to avoid driver titration during epistasis tests. Expression of UAS-PLC δ PHGFP was used to visualize border cell membranes. UAS-Src-CA constructions consisted of a constitutively active form of

Src42A containing a Tyr-Phe substitution at position 511. UAS-GFPnls was used in some epistasis tests to avoid titration of the drivers.

For detailed offspring genotype information for each figure panel, see Table S2.

All crosses and offspring 3- to 4-d old were kept at 25°C. Offspring containing *c306-Gal4* or *slbo-Gal4* driver was transferred to a new vial with dry yeast and shifted to 29°C for 18 h or 24 h, respectively, before dissection. An exception was made with UAS-Src-CA#2 expression where offspring was transferred to a new vial with dry yeast and kept at 25°C for 24 h before dissection. All fly crosses were repeated at least three times.

Transgene verification

UAS-*csk*-RNAi#1 line was created by VDRC using a KK library. The presence of UAS-Inverted Repeated construct in the offspring *mys¹/c306-Gal4*; UAS-*csk*-RNAi#1/UAS-*mys*-RNAi; +/+ was verified by PCR amplification following VDRC protocol. Flies were collected into a 200 μ l PCR tube and mashed with a 200 μ l yellow tip containing 50 μ l squishing buffer (10 mM Tris, 1 mM EDTA, 25 mM NaCl, and 200 g/ml fresh Proteinase K). Then PCR tubes were incubated at 37°C for 30 min, then at 95°C for 2 min, and spun down for 7 min at 14,000 rpm. PCR reactions were set up in 200 μ l PCR tubes with the universal forward primer ETU and specific reverse primer SV2 (see Table S3). PCR reactions (1 cycle of 95°C for 2 min; 38 cycles of 94°C for 30 s, 60°C for 30 s, 72°C for 90 min; and 1 cycle of 72°C for 10 min) were done in the presence of GoTaqGreen master mix (see Table S3) and 1 μ l genomic DNA in a total reaction volume of 20 μ l.

UAS-*mys*-RNAi line, which was also created by VDRC using GD transgenic RNAi library, was used as a negative control as well as *w¹¹¹⁸* fly line. UAS-*csk*-RNAi#1 stock line and the females that were used as parent *mys¹/Fm7*; UAS-*csk*-RNAi#1/UAS-*csk*-RNAi#1; +/+ were used for the positive control. PCR products for the different genotypes were run in a 1.5% agarose gel. GeneRuler 100 bp Plus DNA Ladder was used and a band around 400 base pair indicated the presence of UAS-*csk*-RNAi#1 construct.

Immunostaining

Ovaries extracted from 7–10 adult female flies were dissected in Schneider's *Drosophila* medium supplemented with fetal bovine serum (FBS) and fixed for 15 min in 3.7% formaldehyde at room temperature. Next, they were washed three times (10 min each) with PBT (PBS 1 \times and Triton 4%) and incubated for at least 30 min in PBTA (PBS1X, Triton 4%, and bovine serum albumin 2%) at room temperature. Then, ovaries were incubated in PBTA with primary antibodies for 48 h at 4°C. After this, samples were washed three times (10 min each) with PBT and subsequently incubated in PBTA with secondary antibodies and DAPI for 2 h at room temperature. Finally, samples were washed three times (10 min each) with PBT and mounted on slides with Vectashield mounting medium. For detailed information on antibodies used in this study, see Table S3.

Fas3 prefixed staining

Ovaries extracted from seven adult female flies were dissected in Schneider's *Drosophila* medium supplemented with 20% FBS.

They were next incubated in Schneider's medium with FBS, insulin, and mouse anti-Fas3 antibody for 15 min. They were then washed three times (1 min each) in Schneider's medium with FBS only and fixed for 15 min in 3.7% formaldehyde. Samples were washed three times (10 min each) with PBS 1× and subsequently incubated in PBS 1× with DAPI and the Alexa Fluor goat anti-mouse (568) secondary antibody for 2 h. Finally, samples were washed three times (10 min each) with PBS 1× and mounted in Vectashield mounting medium. All the steps were conducted at room temperature.

LysoTracker staining

LysoTracker Red DND-99 was used following the protocol from [Timmons et al. \(2017\)](#) until the removal of LysoTracker staining. Subsequent fixation and staining steps were performed according to our protocol described earlier.

Egg chamber culture and time-lapse imaging of live egg chambers

Ovaries extracted from three adult female flies expressing lacZ or Src-CA#1 were dissected in Schneider's *Drosophila* medium supplemented with 20% fetal bovine serum. Individual ovarioles were carefully pulled out, and egg chambers after stage 11 were removed. Samples were transferred onto a microglass slide and mounted in 45 µl of dissecting medium containing insulin and DAPI (see concentrations in Table S3) on a Lumox dish sealed with carbon oil to allow for gas exchanges. For detailed information about concentrations, see Table S3. Time-lapse imaging was performed using a 40× 1.4 NA water immersion objective lens. Z-stacks using 0.5–0.8 µm step size were collected at 4-min intervals. Since border cells from egg chambers expressing Src-CA were moving a lot in the z-axis, we had to stop recording very often to refocus and wait for the remaining time between intervals to pass before starting a new series of images. A smooth filter was used for [Videos 6, 7, and 8](#).

Microscopy, image treatment, and quantifications

Images were taken on a Zeiss 800 confocal microscope using a 40× 1.4 N.A. water or 20× 1.2 NA objectives. Z-stacks with optimal resolution were required, in general using a step size between 0.4 and 1 µm. Cluster images were taken using a zoom of 3× or 4×. All confocal images of different genotypes in the same experiment were acquired using the same settings and were performed at 23°C. For high-resolution airyscan imaging, we used a 63× 1.4 N.A. PlanApo oil objective with z-slice thicknesses of 0.16 µm. Airyscan images were collected to examine Rab localization at high spatial resolution and are not suitable for comparison of expression levels.

Confocal imaging stacks were processed with FIJI software ([Schindelin et al., 2012](#)). When Z-slice projections were conducted, the number of slices, the z-step, and the type of projection used were indicated in the legend of the figure. Consecutive time-lapse videos coming from the recording of the same border cell cluster were compiled using the “concatenated” tool from the Stack menu. Egg chambers and clusters from fixed and live images were rotated so that the anterior pole was always pointing left.

IMARIS software (Bitplane) was used to create three-dimensional reconstructions of the polar cells' internalization phenotype from z-stacks of confocal images taken with very good resolution (z-step: 0.5 µm). The surface rendering tool was used to create an accurate 3D structure of individual border cells and polar cells.

For quantification of polar cells' internalization, clusters from egg chambers at stage 10 of oogenesis were analyzed. Border cells were visualized by the expression of UAS-PLCδPHGFP or by E-cadherin (CAD) staining and polar cells by the expression of FAS3. An internalization event per cluster was counted when at least one polar cell or more than half of the polar cell nucleus was inside a border cell (or FC). Quantifications of the phenotype were represented by a bar chart. The values represent the mean of three biological replicates and the error bars corresponded to the standard error of the mean (SEM) using the formula: standard error = STDEV (sampling range)/SQRT (COUNT (sampling range))

For quantifications of pSrc, pSHARK, or pFAK activity, SUM intensity projections (z-step: 0.5 µm) from original z-stack images were created using the same number of slides per genotype. Then, the contour of the border cell clusters (or split clusters) was selected by the freehand selection and the signal from the corresponding channel (pSrc, pSHARK, or pFAK) was measured. Max gray value averages from the control clusters were used to normalize the signal of all genotypes per experiment.

For quantifications of the circularity index, we identified the middle focal plane of each border cell in the z-stack using the endogenous fluorescence of PHGFP. We then selected its contour using the freehand selection and measured its circularity. Fiji calculates circularity using the formula: circularity = $4\pi(\text{area}/\text{perimeter}^2)$, where a value of 1.0 indicates a perfect circle and 0.0 indicates an increasingly elongated polygon. The experiment was done three independent times and the data were shown as boxplots ([Fig. 2 A](#)).

For quantification of border cell migration, different categories were created to classify the position of the cluster in egg chambers at stage 10 of oogenesis: (1) complete migration, (2) incomplete migration, (3) no detachment, and (4) split clusters. “Complete migration” indicates that the cluster reached the oocyte. “Incomplete migration” means the cluster detached from the anterior pole but did not reach the oocyte. “No detachment” means the cluster was still attached to the anterior pole and “split cluster” means at least two border cells have detached from the cluster. Border cell quantifications of the genotypes indicated were graphically represented using bar charts and the values correspond to the mean of three biological replicates. The error bars correspond to the standard error of the mean using the formula previously described for polar cells' internalization quantification.

Statistical analysis

Statistical analysis and box plots were performed with R version 3.6.1. Bar charts were created in Excel. Statistical tests used for each experiment are detailed in each figure legend. All images shown are representative of at least three independent experiments.

Online supplemental material

Fig. S1 shows additional information on polar cell live engulfment, cluster morphology, and migration, and includes information about engulfment at the posterior pole and death of egg chambers overexpressing Src at later stages of oogenesis. **Fig. S2** shows quantifications of pSrc intensities and rescues of cluster cell morphology and border cell migration when hyperactive Src (Src-CA or *cskRNAi*) is expressed in combination with mutant forms of Rac and Rho GTPases, or mutant/knockdown of SHARK and FAK kinases. **Fig. S3** shows additional information about Src signaling through integrins for polar cell engulfment, border cell migration, and cluster morphology. **Video 1** shows a 3D reconstruction of a border cell cluster from an egg chamber at stage 9 expressing LacZ. **Video 2**, **Video 3**, and **Video 4** show 3D reconstructions of border cell clusters from egg chambers at stage 10 expressing Src-CA, where polar cells are being internalized by border cells. **Video 5** shows a time-lapse of the border cell movement without leading protrusions and no detachment from the anterior pole from an egg chamber at stage 10 expressing Src-WT. **Video 6** shows a time-lapse of normal border cell cluster morphology and migration from an egg chamber at stage 10 expressing LacZ. **Video 7** shows polar cell internalization by border cells from an egg chamber at stage 10 expressing Src-CA. **Video 8** shows border cell migration with internalized polar cells from an egg chamber at stage 10 expressing Src-CA. Table S1 shows the effects of the overexpression of different kinases on polar cell engulfment, migration, and morphology of border cell clusters. Table S2 shows the detailed genotypes displayed in each figure. Table S3 shows a list of reagents and resources used.

Acknowledgments

We are grateful to M. Morrissey and J. McDonald for helpful discussions. We are grateful to Dr. T. Kojima (Graduate School of Frontier Sciences, The University of Tokyo, Tokyo, Japan), Prof. C.A. Berg (University of Washington, Seattle, WA, USA), Prof. R. Palmer (Institute of Biomedicine, Sahlgrenska Academy, University of Gothenburg, Gothenburg, Sweden), Prof. C.F. Wu (University of Iowa, Iowa City, IA, USA), Dr. M.R. Freeman (The Vollum Institute, Oregon Health & Science University, Portland, OR, USA), Dr. C.S. Goodman (W.G. (Bill) Hefner VA Medical Center, Salisbury, NC, USA), Prof. A. Nakamura (Institute of Molecular Embryology and Genetics, Kumamoto University, Kumamoto, Japan) for Rab5 antibody (Tanaka et al., 2021), BDSC (Indiana University, Bloomington, IN, USA) and VDRC (Vienna, Austria) for fly stocks as well as to Prof. E.R. Stanley (Albert Einstein College of Medicine, Bronx, NY, USA) for pSHARK (Y927) antibody and to Developmental Studies Hybridoma Bank for providing antibodies. We acknowledge the use of the Imaris computer workstation at the NRI-MCDB Microscopy Facility at UC, Santa Barbara.

We acknowledge funding from the National Institutes of Health (NIH) RO1GM046425.

Author contributions: Conceptualization: A.Y. Torres and D.J. Montell; methodology: A.Y. Torres, M. Nano, J. P. Campanale, and D.J. Montell; investigation: A.Y. Torres, M. Nano, J. P. Campanale, and S. Deak; data curation: A.Y. Torres, M. Nano,

and J. P. Campanale; writing—original draft: A.Y. Torres, M. Nano, and D.J. Montell; writing—edit and review: all authors; supervision: D.J. Montell.

Disclosures: All authors have completed and submitted the ICMJE Form for Disclosure of Potential Conflicts of Interest. A.Y. Torres reported a patent to GENETICALLY ENGINEERED PHAGOCYTES, AND RELATED COMPOSITIONS, VECTORS, METHODS, AND SYSTEMS pending. D.J. Montell reported other from Inceptor Bio outside the submitted work; in addition, D.J. Montell had a patent to 17/995,083 pending “Inceptor Bio.” No other disclosures were reported.

Submitted: 20 February 2023

Revised: 31 July 2023

Accepted: 29 August 2023

References

- Aceto, N., A. Bardia, D.T. Miyamoto, M.C. Donaldson, B.S. Wittner, J.A. Spencer, M. Yu, A. Pely, A. Engstrom, H. Zhu, et al. 2014. Circulating tumor cell clusters are oligoclonal precursors of breast cancer metastasis. *Cell*. 158:1110–1122. <https://doi.org/10.1016/j.cell.2014.07.013>
- Barrett, K., M. Leptin, and J. Settleman. 1997. The Rho GTPase and a putative RhoGEF mediate a signaling pathway for the cell shape changes in *Drosophila* gastrulation. *Cell*. 91:905–915. [https://doi.org/10.1016/s0092-8674\(00\)80482-1](https://doi.org/10.1016/s0092-8674(00)80482-1)
- Biswas, R., D. Stein, and E.R. Stanley. 2006. *Drosophila* Dok is required for embryonic dorsal closure. *Development*. 133:217–227. <https://doi.org/10.1242/dev.02198>
- Borensztein, K., P. Tyrna, A.M. Gaweł, I. Dziuba, C. Wojcik, L.P. Bialy, and I. Mlynarczuk-Bialy. 2021. Classification of cell-in-cell structures: Different phenomena with similar appearance. *Cells*. 10:2569. <https://doi.org/10.3390/cells10102569>
- Bradshaw, J.M. 2010. The src, syk, and tec family kinases: Distinct types of molecular switches. *Cell. Signal*. 22:1175–1184. <https://doi.org/10.1016/j.celsig.2010.03.001>
- Brower, D.L., M. Wilcox, M. Piovant, R.J. Smith, and L.A. Reger. 1984. Related cell-surface antigens expressed with positional specificity in *Drosophila* imaginal discs. *Proc. Natl. Acad. Sci. USA*. 81:7485–7489. <https://doi.org/10.1073/pnas.81.23.7485>
- Brown, G.C., A. Vilalta, and M. Fricker. 2015. Phagoptosis - cell death by phagocytosis - plays central roles in physiology, host defense and pathology. *Curr. Mole. Med.* 15:842–851. <https://doi.org/10.2174/156652401509151105130628>
- Chen, Y.-C., M.E. Gonzalez, B. Burman, X. Zhao, T. Anwar, M. Tran, N. Medhora, A.B. Hizirolu, W. Lee, Y.-H. Cheng, et al. 2019. Mesenchymal stem/stromal cell engulfment reveals metastatic advantage in breast cancer. *Cell Rep*. 27:3916–3926.e5. <https://doi.org/10.1016/j.celrep.2019.05.084>
- Cheung, K.J., V. Padmanaban, V. Silvestri, K. Schipper, J.D. Cohen, A.N. Fairchild, M.A. Gorin, J.E. Verdone, K.J. Pienta, J.S. Bader, and A.J. Ewald. 2016. Polyclonal breast cancer metastases arise from collective dissemination of keratin 14-expressing tumor cell clusters. *Proc. Natl. Acad. Sci. USA*. 113:E854–E863. <https://doi.org/10.1073/pnas.1508541113>
- Desjardins, M., L.A. Huber, R.G. Parton, and G. Griffiths. 1994. Biogenesis of phagolysosomes proceeds through a sequential series of interactions with the endocytic apparatus. *J. Cell Biol.* 124:677–688. <https://doi.org/10.1083/jcb.124.5.677>
- Etchegaray, J.L., A.K. Timmons, A.P. Klein, T.L. Pritchett, E. Welch, T.L. Meehan, C. Li, and K. McCall. 2012. Draper acts through the JNK pathway to control synchronous engulfment of dying germline cells by follicular epithelial cells. *Development*. 139:4029–4039. <https://doi.org/10.1242/dev.082776>
- Finnemann, S.C. 2003. Focal adhesion kinase signaling promotes phagocytosis of integrin-bound photoreceptors. *EMBO J*. 22:4143–4154. <https://doi.org/10.1093/emboj/cdg416>
- Finnemann, S.C., Y. Chang, M. Anand, and M. Sircar. 2007. Integrin receptor-tyrosine kinase signaling cascades that synchronize daily

- RPE phagocytosis of photoreceptor outer segments. *Invest. Ophthalmol. Vis. Sci.* 48:2521.
- Gundem, G., P. Van Loo, B. Kremeyer, L.B. Alexandrov, J.M.C. Tubio, E. Paemmanuil, D.S. Brewer, H.M.L. Kallio, G. Högnäs, M. Annala, et al. 2015. The evolutionary history of lethal metastatic prostate cancer. *Nature*. 520:353–357. <https://doi.org/10.1038/nature14347>
- Gutwillig, A., N. Santana-Magal, L. Farhat-Younis, D. Rasoulouniriana, A. Madi, C. Luxenburg, J. Cohen, K. Padmanabhan, N. Shomron, G. Shapira, et al. 2022. Transient cell-in-cell formation underlies tumor relapse and resistance to immunotherapy. *Elife*. 11:e80315. <https://doi.org/10.7554/eLife.80315>
- Harrison, S.C. 2003. Variation on an src-like theme. *Cell*. 112:737–740. [https://doi.org/10.1016/s0092-8674\(03\)00196-x](https://doi.org/10.1016/s0092-8674(03)00196-x)
- Irby, R.B., and T.J. Yeatman. 2000. Role of Src expression and activation in human cancer. *Oncogene*. 19:5636–5642. <https://doi.org/10.1038/sj.onc.1203912>
- Jipa, A., V. Vedelek, Z. Merényi, A. Ürmösi, S. Takáts, A.L. Kovács, G.V. Horváth, R. Sinka, and G. Juhász. 2021. Analysis of Drosophila Atg8 proteins reveals multiple lipidation-independent roles. *Autophagy*. 17:2565–2575. <https://doi.org/10.1080/15548627.2020.1856494>
- Khammari, A., F. Agnès, P. Gandille, and A.-M. Pret. 2011. Physiological apoptosis of polar cells during Drosophila oogenesis is mediated by Hid-dependent regulation of Diap1. *Cell Death Differ.* 18:793–805. <https://doi.org/10.1038/cdd.2010.141>
- Kim, C., F. Ye, and M.H. Ginsberg. 2011. Regulation of integrin activation. *Annu. Rev. Cell Dev. Biol.* 27:321–345. <https://doi.org/10.1146/annurev-cellbio-100109-104104>
- Kok, S.Y., H. Oshima, K. Takahashi, M. Nakayama, K. Murakami, H.R. Ueda, K. Miyazono, and M. Oshima. 2021. Malignant subclone drives metastasis of genetically and phenotypically heterogeneous cell clusters through fibrotic niche generation. *Nat. Commun.* 12:863. <https://doi.org/10.1038/s41467-021-21160-0>
- Lipsick, J. 2019. A history of cancer research: Tyrosine kinases. *Cold Spring Harb. Perspect. Biol.* 11:a035592. <https://doi.org/10.1101/cshperspect.a035592>
- Llense, F., and E. Martín-Blanco. 2008. JNK signaling controls border cell cluster integrity and collective cell migration. *Curr. Biol.* 18:538–544. <https://doi.org/10.1016/j.cub.2008.03.029>
- Lowell, C.A. 2011. Src-family and syk kinases in activating and inhibitory pathways in innate immune cells: Signaling cross talk. *Cold Spring Harb. Perspect. Biol.* 3:a002352. <https://doi.org/10.1101/cshperspect.a002352>
- Lugini, L., P. Matarrese, A. Tinari, F. Lozupone, C. Federici, E. Iessi, M. Gentile, F. Luciani, G. Parmiani, L. Rivoltini, et al. 2006. Cannibalism of live lymphocytes by human metastatic but not primary melanoma cells. *Cancer Res.* 66:3629–3638. <https://doi.org/10.1158/0008-5472.CAN-05-3204>
- Luo, L., Y.J. Liao, L.Y. Jan, and Y.N. Jan. 1994. Distinct morphogenetic functions of similar small GTPases: Drosophila Drac1 is involved in axonal outgrowth and myoblast fusion. *Genes Dev.* 8:1787–1802. <https://doi.org/10.1101/gad.8.15.1787>
- MacDonald, J.M., M.G. Beach, E. Porpiglia, A.E. Sheehan, R.J. Watts, and M.R. Freeman. 2006. The Drosophila cell corpse engulfment receptor Draper mediates glial clearance of severed axons. *Neuron*. 50:869–881. <https://doi.org/10.1016/j.neuron.2006.04.028>
- Maddipati, R., and B.Z. Stanger. 2015. Pancreatic cancer metastases harbor evidence of polyclonality. *Cancer Discov.* 5:1086–1097. <https://doi.org/10.1158/2159-8290.CD-15-0120>
- Mao, Y., and S.C. Finnemann. 2015. Regulation of phagocytosis by Rho GTPases. *Small GTPases*. 6:89–99. <https://doi.org/10.4161/21541248.2014.989785>
- Martellucci, S., L. Clementi, S. Sabetta, V. Mattei, L. Botta, and A. Angelucci. 2020. Src family kinases as therapeutic targets in advanced solid tumors: What we have learned so far. *Cancers*. 12:1448. <https://doi.org/10.3390/cancers12061448>
- Matsumoto, T., J. Jiang, K. Kiguchi, L. Ruffino, S. Carbajal, L. Beltrán, D.K. Bol, M.P. Rosenberg, and J. DiGiovanni. 2003. Targeted expression of c-Src in epidermal basal cells leads to enhanced skin tumor promotion, malignant progression, and metastasis. *Cancer Res.* 63:4819–4828.
- Meehan, T.L., S.E. Kleinsorge, A.K. Timmons, J.D. Taylor, and K. McCall. 2015. Polarization of the epithelial layer and apical localization of integrins are required for engulfment of apoptotic cells in the Drosophila ovary. *Dis. Model. Mech.* 8:1603–1614. <https://doi.org/10.1242/dmm.021998>
- Metheniti, A., N. Paraskevopoulou, M. Lambropoulou, and V.J. Marmaras. 2001. Involvement of FAK/Src complex in the processes of Escherichia coli phagocytosis by insect hemocytes. *FEBS Lett.* 496:55–59. [https://doi.org/10.1016/s0014-5793\(01\)02405-x](https://doi.org/10.1016/s0014-5793(01)02405-x)
- Mlynarczuk-Bialy, I., I. Dziuba, A. Sarnecka, E. Platos, M. Kowalczyk, K.K. Pels, G.M. Wilczynski, C. Wojcik, and L.P. Bialy. 2020. Entosis: From cell biology to clinical cancer pathology. *Cancers*. 12:E2481. <https://doi.org/10.3390/cancers12092481>
- Mondragon, A.A., A. Yalonetskaya, A.J. Ortega, Y. Zhang, O. Naranjo, J. Elguero, W.-S. Chung, and K. McCall. 2019. Lysosomal machinery drives extracellular acidification to direct non-apoptotic cell death. *Cell Rep.* 27:11–19.e3. <https://doi.org/10.1016/j.celrep.2019.03.034>
- Montell, D.J., W.H. Yoon, and M. Starz-Gaiano. 2012. Group choreography: Mechanisms orchestrating the collective movement of border cells. *Nat. Rev. Mol. Cell Biol.* 13:631–645. <https://doi.org/10.1038/nrm3433>
- Nezis, I.P., B.V. Shrivage, A.P. Sagona, T. Lamark, G. Bjørkøy, T. Johansen, T.E. Rusten, A. Brech, E.H. Baehrecke, and H. Stenmark. 2010. Autophagic degradation of dBruce controls DNA fragmentation in nurse cells during late Drosophila melanogaster oogenesis. *J. Cell Biol.* 190:523–531. <https://doi.org/10.1083/jcb.201002035>
- Niewiadomska, P., D. Godt, and U. Tepass. 1999. DE-Cadherin is required for intercellular motility during Drosophila oogenesis. *J. Cell Biol.* 144:533–547. <https://doi.org/10.1083/jcb.144.3.533>
- Nonaka, S., K. Nagao, T. Mori, A. Shiratsuchi, and Y. Nakanishi. 2013. Integrin α PS3/ β v-mediated phagocytosis of apoptotic cells and bacteria in Drosophila. *J. Biol. Chem.* 288:10374–10380. <https://doi.org/10.1074/jbc.M113.451427>
- Overholtzer, M., A.A. Mailleux, G. Mounneime, G. Normand, S.J. Schnitt, R.W. King, E.S. Cibas, and J.S. Brugge. 2007. A nonapoptotic cell death process, entosis, that occurs by cell-in-cell invasion. *Cell*. 131:966–979. <https://doi.org/10.1016/j.cell.2007.10.040>
- Pedraza, L.G., R.A. Stewart, D.-M. Li, and T. Xu. 2004. Drosophila Src-family kinases function with Csk to regulate cell proliferation and apoptosis. *Oncogene*. 23:4754–4762. <https://doi.org/10.1038/sj.onc.1207635>
- Roskoski, R., Jr. 2015. Src protein-tyrosine kinase structure, mechanism, and small molecule inhibitors. *Pharmacol. Res.* 94:9–25. <https://doi.org/10.1016/j.phrs.2015.01.003>
- Scheib, J.L., C.S. Sullivan, and B.D. Carter. 2012. Jedi-1 and MEGF10 signal engulfment of apoptotic neurons through the tyrosine kinase Syk. *J. Neurosci.* 32:13022–13031. <https://doi.org/10.1523/JNEUROSCI.6350-11.2012>
- Schindelin, J., I. Arganda-Carreras, E. Frise, V. Kaynig, M. Longair, T. Pietzsch, S. Preibisch, C. Rueden, S. Saalfeld, B. Schmid, et al. 2012. Fiji: An open-source platform for biological-image analysis. *Nat. Methods*. 9:676–682. <https://doi.org/10.1038/nmeth.2019>
- Serizier, S.B., J.S. Peterson, and K. McCall. 2022. Non-autonomous cell death induced by the Draper phagocytosis receptor requires signaling through the JNK and SRC pathways. *J. Cell Sci.* 135:jcs250134. <https://doi.org/10.1242/jcs.250134>
- Shvartsman, D.E., J.C. Donaldson, B. Diaz, O. Gutman, G.S. Martin, and Y.I. Henis. 2007. Src kinase activity and SH2 domain regulate the dynamics of Src association with lipid and protein targets. *J. Cell Biol.* 178:675–686. <https://doi.org/10.1083/jcb.200701133>
- Sicheri, F., and J. Kuriyan. 1997. Structures of Src-family tyrosine kinases. *Curr. Opin. Struct. Biol.* 7:777–785. [https://doi.org/10.1016/s0959-440x\(97\)80146-7](https://doi.org/10.1016/s0959-440x(97)80146-7)
- Song, Z., K. McCall, and H. Steller. 1997. DCP-1, a Drosophila cell death protease essential for development. *Science*. 275:536–540. <https://doi.org/10.1126/science.275.5299.536>
- Springer, T.A., and M.L. Dustin. 2012. Integrin inside-out signaling and the immunological synapse. *Curr. Opin. Cell Biol.* 24:107–115. <https://doi.org/10.1016/j.ceb.2011.10.004>
- Stewart, R.A., D.-M. Li, H. Huang, and T. Xu. 2003. A genetic screen for modifiers of the lats tumor suppressor gene identifies C-terminal Src kinase as a regulator of cell proliferation in Drosophila. *Oncogene*. 22:6436–6444. <https://doi.org/10.1038/sj.onc.1206820>
- Sun, H., K. Zhi, L. Hu, and Z. Fan. 2021. The activation and regulation of β 2 integrins in phagocytes and phagocytosis. *Front. Immunol.* 12:633639. <https://doi.org/10.3389/fimmu.2021.633639>
- Sun, Q., E.S. Cibas, H. Huang, L. Hodgson, and M. Overholtzer. 2014. Induction of entosis by epithelial cadherin expression. *Cell Res.* 24:1288–1298. <https://doi.org/10.1038/cr.2014.137>
- Takahashi, F., S. Endo, T. Kojima, and K. Saigo. 1996. Regulation of cell-cell contacts in developing Drosophila eyes by Dsrc41, a new, close relative of vertebrate c-src. *Genes Dev.* 10:1645–1656. <https://doi.org/10.1101/gad.10.13.1645>
- Takáts, S., P. Nagy, Á. Varga, K. Pircs, M. Kárpáti, K. Varga, A.L. Kovács, K. Hegedűs, and G. Juhász. 2013. Autophagosomal Syntaxin17-dependent lysosomal degradation maintains neuronal function in Drosophila. *J. Cell Biol.* 201:531–539. <https://doi.org/10.1083/jcb.201211160>

- Tanaka, T., N. Tani, and A. Nakamura. 2021. Receptor-mediated yolk uptake is required for oskar mRNA localization and cortical anchorage of germ plasm components in the *Drosophila* oocyte. *PLoS Biol.* 19:e3001183. <https://doi.org/10.1371/journal.pbio.3001183>
- Thomas, S.M., and J.S. Brugge. 1997. Cellular functions regulated by Src family kinases. *Annu. Rev. Cell Dev. Biol.* 13:513–609. <https://doi.org/10.1146/annurev.cellbio.13.1.513>
- Timmons, A.K., A.A. Mondragon, T.L. Meehan, and K. McCall. 2017. Control of non-apoptotic nurse cell death by engulfment genes in *Drosophila*. *Fly.* 11:104–111. <https://doi.org/10.1080/19336934.2016.1238993>
- Torres, A.Y., M. Malartre, A.-M. Pret, and F. Agnès. 2017. JAK/STAT signaling is necessary for cell monosis prior to epithelial cell apoptotic extrusion. *Cell Death Dis.* 8:e2814. <https://doi.org/10.1038/cddis.2017.166>
- Torres-Gomez, A., C. Cabañas, and E.M. Lafuente. 2020. Phagocytic integrins: Activation and signaling. *Front. Immunol.* 11:738. <https://doi.org/10.3389/fimmu.2020.00738>
- Turro, E., D. Greene, A. Wijgaerts, C. Thys, C. Lentaigine, T.K. Bariana, S.K. Westbury, A.M. Kelly, D. Selleslag, J.C. Stephens, et al. 2016. A dominant gain-of-function mutation in universal tyrosine kinase SRC causes thrombocytopenia, myelofibrosis, bleeding, and bone pathologies. *Sci. Transl. Med.* 8:328ra30. <https://doi.org/10.1126/scitranslmed.aad7666>
- Ueda, A., C. Grabbe, J. Lee, J. Lee, R.H. Palmer, and C.-F. Wu. 2008. Mutation of *Drosophila* focal adhesion kinase induces bang-sensitive behavior and disrupts glial function, axonal conduction and synaptic transmission. *Eur. J. Neurosci.* 27:2860–2870. <https://doi.org/10.1111/j.1460-9568.2008.06252.x>
- Uribe-Querol, E., and C. Rosales. 2020. Phagocytosis: Our current understanding of a universal biological process. *Front. Immunol.* 11:1066. <https://doi.org/10.3389/fimmu.2020.01066>
- van Oers, N.S., N. Killeen, and A. Weiss. 1996. Lck regulates the tyrosine phosphorylation of the T cell receptor subunits and ZAP-70 in murine thymocytes. *J. Exp. Med.* 183:1053–1062. <https://doi.org/10.1084/jem.183.3.1053>
- Vieira, O.V., C. Bucci, R.E. Harrison, W.S. Trimble, L. Lanzetti, J. Gruenberg, A.D. Schreiber, P.D. Stahl, and S. Grinstein. 2003. Modulation of Rab5 and Rab7 recruitment to phagosomes by phosphatidylinositol 3-kinase. *Mol. Cell. Biol.* 23:2501–2514. <https://doi.org/10.1128/MCB.23.7.2501-2514.2003>
- Wetzel, D.M., E.L. Rhodes, S. Li, D. McMahon-Pratt, and A.J. Koleske. 2016. The src kinases hck, fgr and lyn activate arg to facilitate IgG-mediated phagocytosis and leishmania infection. *J. Cell Sci.* 129:3130–3143. <https://doi.org/10.1242/jcs.185595>
- Wheeler, D.L., M. Iida, and E.F. Dunn. 2009. The role of Src in solid tumors. *Oncologist.* 14:667–678. <https://doi.org/10.1634/theoncologist.2009-0009>
- Wu, H.-H., E. Bellmunt, J.L. Scheib, V. Venegas, C. Burkert, L.F. Reichardt, Z. Zhou, I. Fariñas, and B.D. Carter. 2009. Glial precursors clear sensory neuron corpses during development via Jedi-1, an engulfment receptor. *Nat. Neurosci.* 12:1534–1541. <https://doi.org/10.1038/nn.2446>
- Yang, Y.-Q., and J.-C. Li. 2012. Progress of research in cell-in-cell phenomena. *Anat. Rec.* 295:372–377. <https://doi.org/10.1002/ar.21537>
- Zheng, X.M., R.J. Resnick, and D. Shalloway. 2000. A phosphotyrosine displacement mechanism for activation of Src by PTPalpha. *EMBO J.* 19:964–978. <https://doi.org/10.1093/emboj/19.5.964>
- Ziegenfuss, J.S., R. Biswas, M.A. Avery, K. Hong, A.E. Sheehan, Y.-G. Yeung, E.R. Stanley, and M.R. Freeman. 2008. Draper-dependent glial phagocytic activity is mediated by Src and Syk family kinase signalling. *Nature.* 453:935–939. <https://doi.org/10.1038/nature06901>

Supplemental material

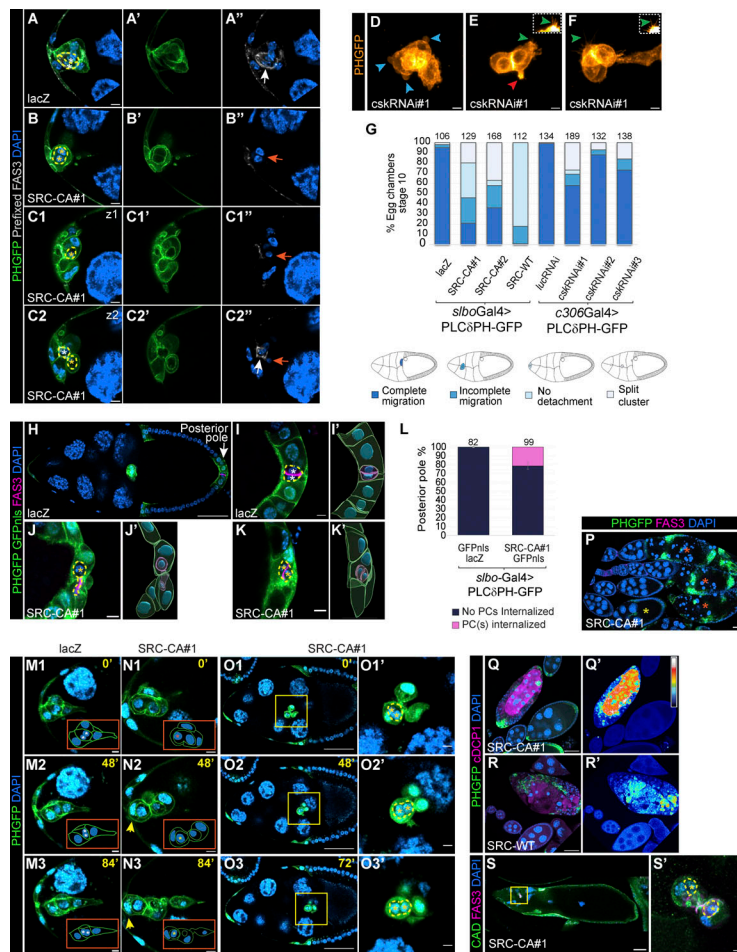


Figure S1. Elevated SRC activity promotes the engulfment of living polar cells and alters cluster morphology and migration. (A–C2’) Confocal images of border cell clusters from egg chambers in stage 9 or 10 expressing UAS-PLC δ PHGFP and the genotypes indicated. Egg chambers were incubated with FAS3 (gray) antibody before fixation and without permeabilization treatment (see Materials and methods). A is a maximal projection of 10 slices (z-step: 0.4 μ m). White asterisk in A and C2 indicates non-internalized polar cells. Yellow asterisks in B–C2 indicate partially/fully internalized polar cells. White arrows in A’ and C2’ point to FAS3 accumulation in non-internalized polar cells and orange ones in B’–C2’ point to the absence of FAS3 due to polar cell internalization by border cells. (C1–C1’) and (C2–C2’) are single sections of two different focal planes of the same cluster. Scale bar: 5 μ m. **(D–F)** Maximum intensity projection from three slices (z-step: 0.5 μ m) of border cell clusters expressing UAS-PLC δ PHGFP and UAS-*cskRNAi#1*. Blue, red, and green arrowheads point to blebs, thick protrusions, and filipodia, respectively. Scale bar: 5 μ m. Insets in E and F show a crop with increased intensity for PLC δ PHGFP from the corresponding images, allowing the observation of filipodia structures. **(G)** Quantification of border cell migration of egg chambers at stage 10 for the genotypes indicated. The total number of samples is indicated at the top of each bar. Four categories were established and represented with a scheme at the bottom of the bar graph (see Materials and methods). **(H)** Single section from confocal images of an egg chamber at stage 10 expressing UAS-PLC δ PHGFP, UAS-GFPnls, and UAS-lacZ. Egg chamber was stained with FAS3 (magenta) and DAPI (blue). Posterior pole is labeled and indicated by a white arrow. Scale bar, 50 μ m. **(I–K)** Single section from confocal images of the posterior pole from egg chambers at stage 10 expressing UAS-PLC δ PHGFP, UAS-GFPnls, and the genotypes indicated. White asterisks in I indicate non-internalized polar cells. Yellow asterisks in J and K indicate polar cells that were internalized by FC. Scale bar, 5 μ m. **(I’–K’)** 3D reconstructions of the respective images are shown in I–K. **(L)** Quantifications of posterior polar cells internalization from egg chambers at stage 10 of the indicated genotypes (see Materials and methods). The total number of samples is indicated at the top of each bar. **(M–O3’)** Single sections from confocal live imaging of border cell clusters from stage 9 or 10 egg chambers expressing UAS-PLC δ PHGFP and the genotypes indicated. DAPI was added to the medium to visualize DNA (see Materials and methods). M1–M3 and N1–N3 are still images at 0, 48, and 84 min of Videos 6 and 7, respectively. Orange insets are schematic representations of the images shown. O1–O3 are time-lapse images at 0, 48, and 72 min of Video 8. White asterisks indicate non-internalized polar cells and orange or yellow asterisks indicate partially or fully internalized polar cells, respectively. Yellow arrows in N2 and N3 point to a border cell containing one polar cell. O1–O3 are time-lapse images at 0, 48, and 72 min of Video 8. Yellow insets in O1–O3 frame border cell clusters and their respective crop images are exhibited in O1’–O3’. A smooth filter was applied to the images. Scale bar in M1–N3, and O1–O3: 5 μ m. Scale bar in O1’–O3’: 50 μ m. **(P)** Maximal projection from 10 slices (z-step: 1.5 μ m) of confocal images of egg chambers expressing UAS-PLC δ PHGFP and UAS-SRC-CA#1. Egg chambers were stained with FAS3 (magenta). DNA is visualized by DAPI (blue). Yellow asterisk indicates a living stage 10 egg chamber and orange asterisks indicate dying egg chambers at later stages of oogenesis. Scale bar: 50 μ m. **(Q–R)** Maximum intensity projection from five slices (z-step: 0.5 μ m) of egg chambers in stage 9 or 10 expressing UAS-PLC δ PHGFP and the genotypes indicated. Egg chambers were stained with cDCP1 (magenta) and DAPI (blue). Scale bar: 50 μ m. **(Q’–R’)** Images from Q–R showing only cDCP1 staining in Royal LUT where white represents the highest amount of cDCP1 and black the lowest one. **(S and S’)** Maximal projection of 10 slices from confocal images of an egg chamber at stage 14 (z-step: 0.9 μ m) expressing UAS-PLC δ PHGFP and UAS-SRC-CA#1, and its respective border cell cluster framed by a yellow insert (z-step: 0.4 μ m) and shown at a higher magnification in S’. Egg chambers were stained with CAD (green) and FAS3 (magenta). DNA is visualized by DAPI (blue). Yellow asterisks in R’ label internalized polar cells. Polar cells in panels A–C2, I–K, and S are outlined with a yellow dashed line.

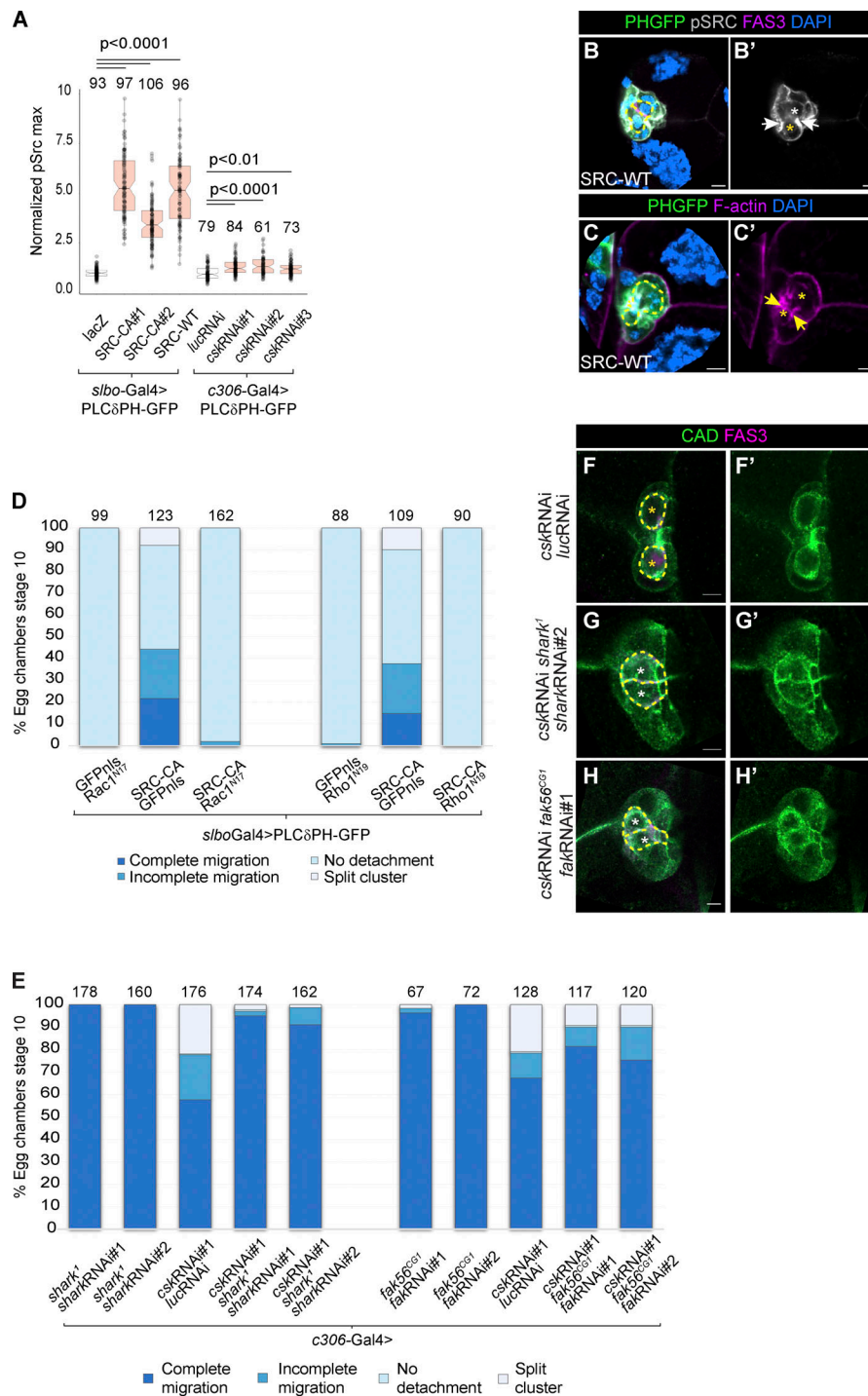


Figure S2. Rac, Rho, SHARK, and FAK are required for activated SRC to affect border cell migration and morphology. (A) Quantifications of normalized pSRC maximal intensity from egg chambers in stage 9 or 10 of the indicated genotypes (see Materials and methods). Box plots are used to represent the data. Each box plot shows the median (line) with 25th and 75th percentiles (hinges) plus 1.5 \times interquartile ranges (whiskers). Dots represent each cluster analyzed and their total number per genotype (n) is indicated on the top of each box plot. Normal distribution was tested using Kolmogorov-Smirnov test. Since data were normally distributed, an ANOVA test (one-tailed) with post-hoc Tukey was performed to evaluate statistical significance. P values are shown at the top of the graph. (B-C) Maximum intensity projection from three slices (z -step: 0.5 μ m) of border cell clusters expressing UAS-PLC δ PHGFP and UAS-SRC-WT. Egg chambers were stained with pSRC (gray) and FAS3 (magenta) in B and B', and with F-actin (magenta) in C and C'. DNA is visualized by DAPI (blue). White asterisks in B and B' indicate non-internalized polar cells and yellow ones in B-C' indicate partially internalized polar cells. White arrows in B' point to pSRC accumulation, and yellow arrows in C' point to F-actin accumulation. Scale bar: 5 μ m. (D and E) Quantification of border cell migration in stage 10 egg chambers for the genotypes indicated (see Materials and methods). The total number of samples is indicated on top of each bar. (F-H) Single sections of border cell clusters from stage 10 egg chambers expressing the genotypes indicated. Egg chambers were stained with CAD (green) and FAS3 (magenta). Yellow asterisks in F indicate internalized polar cells and white ones in G and H indicate non-internalized polar cells. Polar cells are outlined with a yellow dashed line. Scale bar: 5 μ m.

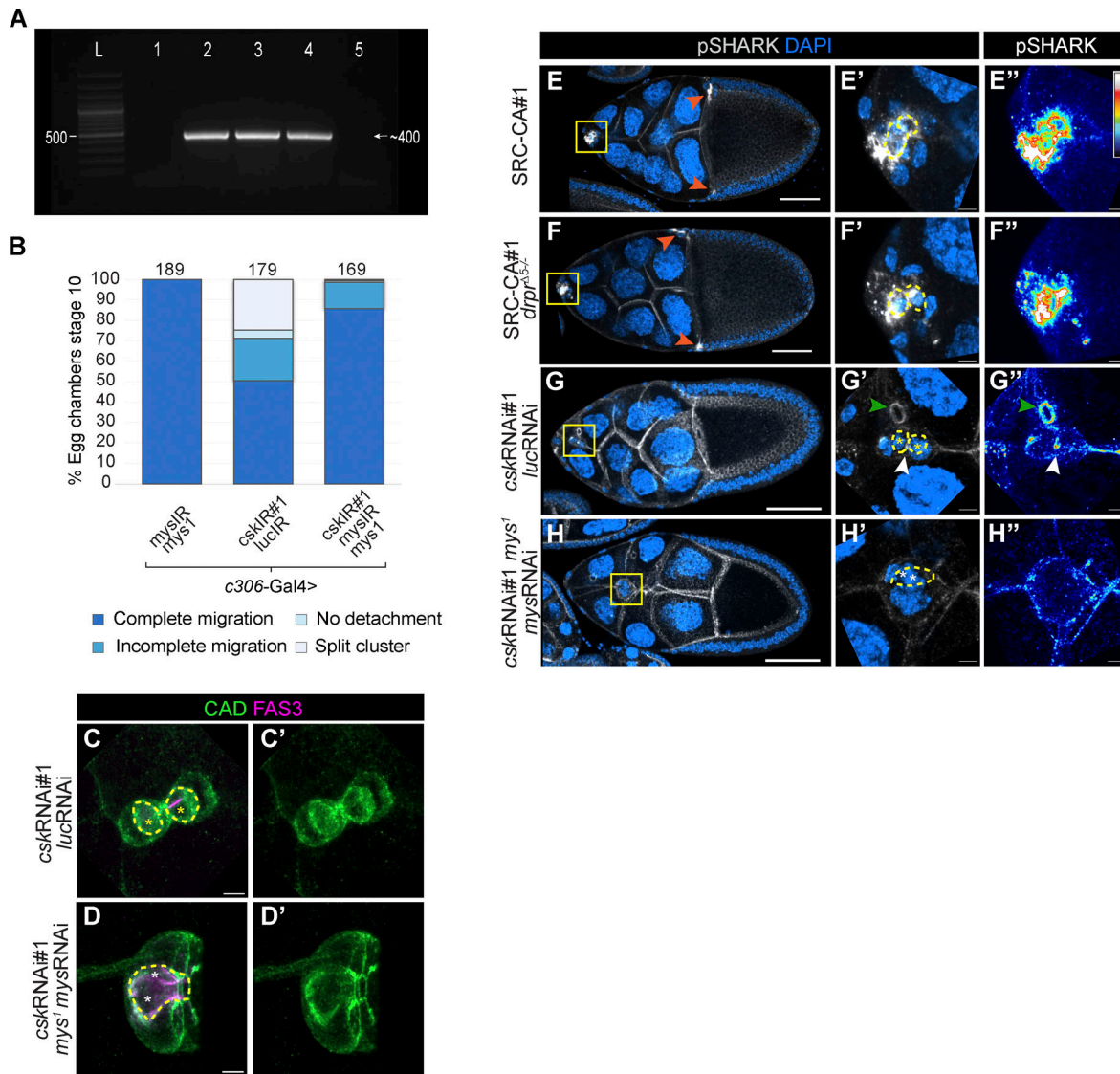


Figure S3. **SRC is upstream of β PS integrin subunit for polar cell engulfment, border cell migration, and cell cluster morphology.** (A) Verification by polymerase chain reaction of the presence of *csk* inverted repeated sequence which is indicated by a band of ~400 base pairs (see Materials and methods). "L" indicates Ladder; (1) *w¹¹¹⁸*, (2) *cskRNAi*, (3) *mys¹*; *cskRNAi*, (4) *mys¹/c306-Gal4*; *cskRNAi/mysRNAi*, (5) *mysRNAi* (see Table S1 to specific genotypes). (B) Quantification of border cell migration of egg chambers at stage 10 for the genotypes indicated (see Materials and methods). The total number of samples is indicated on top of each bar. (C-D') Maximum intensity projection from seven slices (z-step: 0.6 μ m) of confocal images of border cell clusters from stage 10 egg chambers expressing the genotypes indicated. Egg chambers were stained with CAD (green) and FAS3 (magenta). Yellow asterisks in C indicate internalized polar cells and white ones in (D) indicate non-internalized polar cells. Scale bar: 5 μ m. (E-H') Maximum intensity projection from six slices (z-step: 1 μ m) (E-F') or 20 slices (z-step: 0.5 μ m) (G-H') of confocal images of egg chambers at stage 10 (E-F') or stage 9 (G-H') expressing the genotypes indicated. (E'-H') magnify the insets in E-H. Egg chambers were stained with pSHARK (pY927; gray) and DAPI (blue). pSHARK accumulation in centripetal cells is labeled by orange arrows in E-F. (E''-H'') Same images are shown in E'-H' where pSHARK staining is shown in a Royal LUT. White represents the highest amount of protein and black the lowest one. White arrows in G' and G'' point to pSHARK accumulation and green arrowheads point to a ring canal enriched in pSHARK. Scale bar: 50 μ m in E-H and 5 μ m in E'-H''. Polar cells in panels C-D and E'-H' are outlined with a yellow dashed line. White or yellow asterisks indicate non-internalized or fully internalized polar cells, respectively.

Video 1. **3D reconstruction of a border cell cluster from an egg chamber at stage 9 expressing *slbo-Gal4>UAS-lacZ/UAS-PLC δ PHGFP***. Polar cells are identified by FAS3 (magenta) and are surrounded by the border cells (green). Nuclei are shown in blue. Related to Fig. 1, F and F'.

Video 2. **3D reconstruction of a border cell cluster from an egg chamber at stage 10 expressing *slbo-Gal4>UAS-SRC-CA#1; UAS-PLCδPHGFP*.** Polar cells are identified by FAS3 (magenta) and they are being squeezed by border cells (green). Nuclei are shown in blue. Related to [Fig. 1, H and H'](#).

Video 3. **3D reconstruction of a border cell cluster from an egg chamber at stage 10 expressing *slbo-Gal4>UAS-SRC-CA#1; UAS-PLCδPHGFP*.** Polar cells are identified by FAS3 (magenta) and each polar cell has been internalized by two different border cells (green). Nuclei are shown in blue. Related to [Fig. 1, I and I'](#).

Video 4. **3D reconstruction of a border cell cluster from an egg chamber at stage 10 expressing *slbo-Gal4>UAS-SRC-CA#1; UAS-PLCδPHGFP*.** Polar cells are identified by FAS3 (magenta) and border cells are in green. Both polar cells have been internalized by only one border cell. Nuclei are shown in blue. Related to [Fig. 1, J and J'](#).

Video 5. **Time-lapse showing the movement of the border cell cluster without leading protrusions and no detachment from the anterior pole.** Maximal projection from 20 slices (z-step: 0.7 μm) of confocal images of an egg chamber at stage 10 expressing *slbo-Gal4>UAS-SRC-WT/UAS-PLCδPHGFP*. DAPI was added to the medium to identify nuclei (see Materials and methods).

Video 6. **Time-lapse showing normal border cell cluster morphology and migration.** Maximal projection from 40 slices (z-step: 0.8 μm) of confocal images of egg chambers expressing *slbo-Gal4>UAS-lacZ/UAS-PLCδPHGFP*. DAPI was added to the medium to identify nuclei (see Materials and methods). Related to [Fig. S1, M1–M3](#).

Video 7. **Time-lapse showing polar cells internalization by border cells.** Maximal projection from 43 slices (z-step: 0.5 μm) of confocal images of egg chambers expressing *slbo-Gal4>UAS-SRC-CA#1; UAS-PLCδPHGFP*. DAPI was added to the medium to identify nuclei (see Materials and methods). Related to [Fig. S1, N1–N3](#).

Video 8. **Time-lapse showing border cell migration with internalized polar cells.** Single section of border cells from egg chambers expressing *slbo-Gal4>UAS-SRC-CA#1; UAS-PLCδPHGFP/UAS-GFPnls*. DAPI was added to the medium to identify nuclei (see Materials and methods). Related to [Fig. S1, O1–O3'](#).

Provided online are [Table S1](#), [Table S2](#), and [Table S3](#). [Table S1](#) shows a list of overexpressed kinases and corresponding phenotypes. [Table S2](#) shows detailed genotypes displayed in each figure. [Table S3](#) shows a list of reagents and resources used in this study.